5-2011

Pleistocene climate in Alaska from stable isotopes in an ice wedge

Corinne Y. Griffing
University of Nevada, Las Vegas

PLEISTOCENE CLIMATE IN ALASKA FROM STABLE ISOTOPES IN AN ICE WEDGE

by

Corinne Yvonne Griffing

Bachelor of Science
University of Nevada, Las Vegas
2008

A thesis submitted in partial fulfillment
of the requirements for the

Master of Science in Geoscience
Department of Geoscience
College of Science

Graduate College
University of Nevada, Las Vegas
May 2011

THE GRADUATE COLLEGE

We recommend the thesis prepared under our supervision by

Corinne Y. Griffing

entitled

Pleistocene Climate in Alaska from Stable Isotopes in an Ice Wedge

be accepted in partial fulfillment of the requirements for the degree of

Master of Science in Geoscience

Matthew Lachniet, Committee Chair

Daniel Lawson, Committee Member

Ganqing Jiang, Committee Member

Stephen Rowland, Committee Member

Liam Frink, Graduate Faculty Representative

Ronald Smith, Ph. D., Vice President for Research and Graduate Studies
and Dean of the Graduate College

May 2011

ABSTRACT

Pleistocene Climate in Alaska from Stable Isotopes in an Ice Wedge

by

Corinne Y. Griffing

Dr. Matthew Lachniet, Examination Committee Chair
Associate Professor of Geology
University of Nevada, Las Vegas

The CRREL permafrost tunnel offers a unique opportunity to sample ice wedges in a climate-controlled environment, penetrating frozen silts which host massive ground ice that may record Dansgaard-Oeschger (D-O) and Heinrich Events. Ice wedges in the tunnel have been dated to approximately 36-22 ka (Hamilton et al., 1988), allowing the paleoclimate of the region to be reconstructed during MIS 3, when D-O and Heinrich events were documented in various other records. These climate cycles are rapid climate oscillations that have been recognized in records from the Arctic and subarctic, and suggest that climate can rapidly shift by 10°C over millennial scale times. I hypothesize that climate in the interior of Alaska varied with Heinrich events during MIS 3, and that these events were recorded as stable isotope variations in local permafrost ground ice. To test this hypothesis, I sampled an ice wedge in the permafrost tunnel for $\delta^{18}O$, δD and ^{14}C to obtain a detailed climate record from central Alaska.

$\delta^{18}O$ values from within the wedge display a gradual decrease of 5.95‰ from the center toward the left edge, interpreted to reflect decreasing temperature, and is the same magnitude of decrease seen during the transition from the warm D-O interstadial 5 to the cold of Heinrich Event 3 in the NGRIP record in Greenland. Radiocarbon dates from within the wedge range from 28 – 37 cal kyr BP, and are interpreted here not to be the

same age as the ice, but rather represent warm periods when sediment aggraded prior to ice wedge growth. These results suggest that D-O and Heinrich events impacted Late Pleistocene climate and ground ice in central Alaska.

TABLE OF CONTENTS

LIST OF FIGURES

CHAPTER 1

INTRODUCTION

High latitude regions are highly sensitive indicators of and reactors to climate change, making them ideal field laboratories for studying climate fluctuations (Anisimov et al., 2007). An understanding of how climate in high latitude regions has responded to rapid fluctuations in the past is useful for evaluating modern changes in climate, and predictions for future change. Because there are few long-term climate records in central Alaska, millennial scale climate oscillations have not been clearly documented in this region. This study seeks to identify such climatic variations in ground ice near Fairbanks, Alaska.

Two large, rapid climate change events seen in multiple records are Dansgaard-Oeschger (D-O) cycles and Heinrich events (Figure 1). D-O events show large temperature increases of up to 10°C over short intervals of a few thousand years during Marine Isotope Stage 3 (MIS 3), between ~11 and 100 thousand years ago (ka) (Dansgaard et al., 1993). D-O events were first recognized by Dansgaard et al. (1993) in the GRIP ice core in Greenland, which provided a climate record spanning the last 250 ka using oxygen isotope ratios. Interstadials, identified by maximum $\delta^{18}O$ values, are numbered 1-24 (Figure 1) (Dansgaard et al., 1993; Schultz, 2002). Similar large and abrupt shifts in temperature were identified in North Atlantic ocean cores by Bond et al. (1993), who used planktic foraminifera as a proxy for sea surface temperature in a record covering the past 90 ka. Since that time, D-O events have been identified in records around the globe (e.g. Asmerom et al., 2010; Behl and Kennett, 1996; Cosford et al., 2008).

Heinrich events are cool periods recorded during the last glaciation, thought to be caused by armadas of icebergs produced by massive calving of the Laurentide Ice Sheet (Bond et al., 1993; Bond et al., 1999). The events were documented in part by foraminifera evidence of an influx of fresh water into the North Atlantic and anomalous layers of ice-rafted detritus (IRD) in ocean sediment cores (Hemming, 2004). Heinrich events often immediately precede D-O events, and the two climate fluctuations have been demonstrated to be closely related (Bond et al., 1993). D-O cycles are thought to be the result of oscillations in the North Atlantic's thermohaline circulation, caused by changes in the ocean's salinity (Broecker et al., 1990). Freshwater input is necessary to decrease the salinity of the North Atlantic, and the large iceberg discharges associated with Heinrich events are large enough to influence circulation of the ocean (Bond et al., 1999). Various suggestions regarding the cause of large iceberg calving events from the Laurentide Ice Sheet involve the internal oscillatory dynamics of ice sheets (Bond et al., 1993), and a possible response to the cold phases of D-O cycles (Bond and Lotti, 1995).

Millennial scale climate change events have been identified in multiple records from high latitude regions. In the North Pacific, studies of the abundance of foraminifera and fluctuations of IRD at Ocean Drilling Program (ODP) Site 883 (located at 51°N) have indicated D-O and Heinrich events, with sea surface temperature (SST) fluctuations of 2.5° – 4°C (Kiefer et al., 2001; Kotilainen and Shackleton, 1995). In the middle latitudes, oxygen isotope records from stalagmites in Hulu Cave in China record Asian Monsoon Interstadials, which have been linked to D-O interstadials and Heinrich events (Wang et al., 2001). SST warmings of 3° – 5°C associated with D-O cycles are inferred from foraminiferal assemblage changes at ODP Site 893A in the Santa Barbara basin (Hendy

and Kennett, 1999). Similar millennial scale climate change events, including a possible Younger Dryas event, have been identified in a 250 thousand year (kyr) long paleoclimate record from El'gygytgyn Crater Lake in northeastern Siberia (Brigham-Grette et al., 2007). The Younger Dryas occurred between 12.9 and 11.5 ka, and was an abrupt large scale cooling event documented in various climate records (Broecker et al., 1989, Meyer et al., 2010). In Alaska, the Younger Dryas event has recently been recognized in lake sediment records in the south-central part of the state as well as from ground ice records on the North Slope (Kaufman et al., 2010; Meyer et al., 2010).

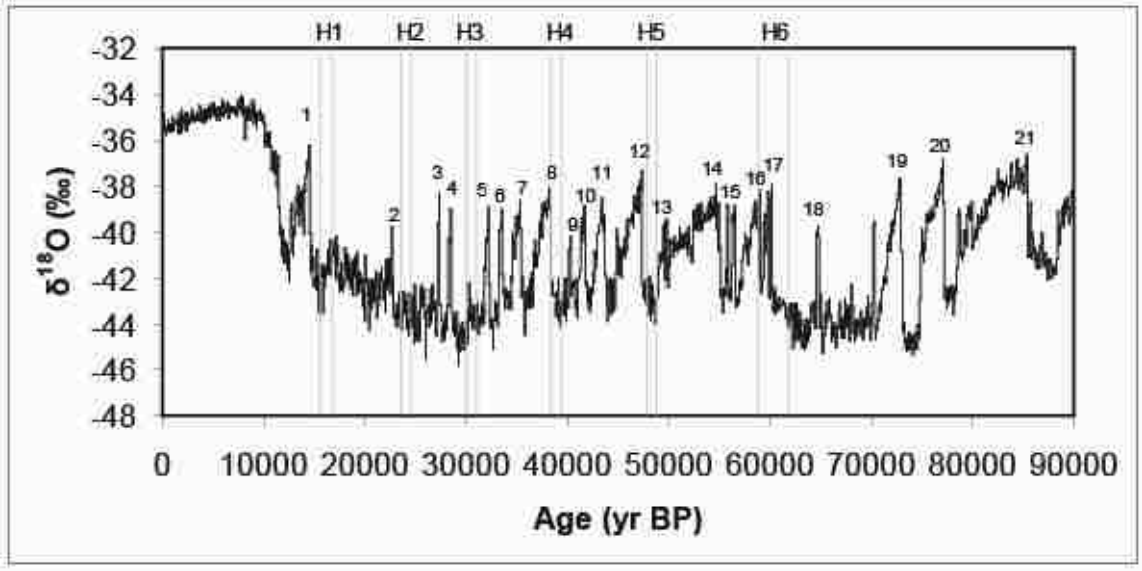

Figure 1. $\delta^{18}O$ record from NGRIP with 50-year resolution. Numbers 1-21 identify Greenland interstadials associated with D-O events; boxes labeled H1-H6 are Heinrich events as dated from Hulu Cave (Wang et al., 2001).

The Arctic region is characterized by a relative scarcity of paleoclimate records, particularly terrestrial, covering MIS 3 (Voelker, 2002). The majority of records spanning this time are from marine sites, and terrestrial records are generally from lower and

middle latitudes. Few records in Alaska have sufficient temporal resolution or length to show millennial scale oscillations, and those in Alaska that do show apparent cycles have not clearly been correlated to D-O or Heinrich events (e.g. Anderson et al., 1994; Beget, 1996; Eisner and Colinvaux, 1990). This raises the question of whether central Alaska experienced these significant changes in temperature.

The aim of this project was to identify and study climatic events in a high latitude terrestrial record, specifically in central Alaska, utilizing stable isotope measurements from relict ground ice in Fox, Alaska. If events of Younger Dryas magnitude were documented across Alaska in multiple proxies, D-O events would likely also be recorded. Since much of Central Alaska was not glaciated during MIS 3, and few lakes in the region offer detailed records of sufficient temporal length, other climate proxies must be used. Previous terrestrial studies spanning MIS 3 have included evaluation of proxy records including loess deposits, ground ice, lake sediments, and other Late Quaternary records (e.g. Anderson and Brubaker, 1994; Axford et al., 2009; Beget et al., 1990; Eisner and Colinvaux, 1990). Ice wedges within permafrost are one proxy in Central Alaska from which oxygen and hydrogen isotope data can be obtained, providing information about past temperature and precipitation (Meyer et al., 2010; Vasil'chuk and Vasil'chuk, 1997)

CHAPTER 2

BACKGROUND

Geologic Background

The Cold Regions Research and Engineering Laboratory (CRREL) permafrost tunnel (CPT) is located in Fox, Alaska, approximately 15 km north of Fairbanks in the Goldstream Valley near the southern limit of the Yukon-Tanana Upland (64°57.084' N, 147°37.250' W) (Figure 2). The tunnel accesses a sequence of Late-Pleistocene-age silt, re-transported loess, and alluvium that overlies schistose bedrock. It was excavated in multiple stages between 1963 and 1969, primarily by CRREL and the U.S. Bureau of Mines (Hamilton et al., 1988). The length of the tunnel is approximately 110 m, and consists of a horizontal adit, a vertical ventilation shaft, and a descending winze providing access to lower silt sections and bedrock (Figure 3).

In the Goldstream Valley, the bedrock is Precambrian Birch Creek Schist, exposure of which is limited to the lower 0.5 – 1 m of the walls at the bottom of the winze in the tunnel (Hamilton et al., 1988; Sellmann, 1967). The bedrock is unconformably overlain by the perennially frozen Fox Gravel, which formed during glacial intervals when solifluction deposits were produced on hillsides and accumulated in valley bottoms (Pewe 1975). The Fox Gravel underlies the Goldstream Formation, the contact of which was dated by Long (1996) to 43,410 ± 240 years, and 39,000 – 46,000 years by Hamilton et al. (1998). The Goldstream Formation is composed of two organic rich silt units. The majority of segregated ice and massive ice structures are located in the Goldstream Formation. The lower unit is 4.5 m thick within the permafrost tunnel, and consists of

well-sorted coarse to medium silt, and the upper unit is approximately 8-11 m thick in the tunnel exposure, consisting of well-sorted coarse to medium silt (Hamilton et al., 1988).

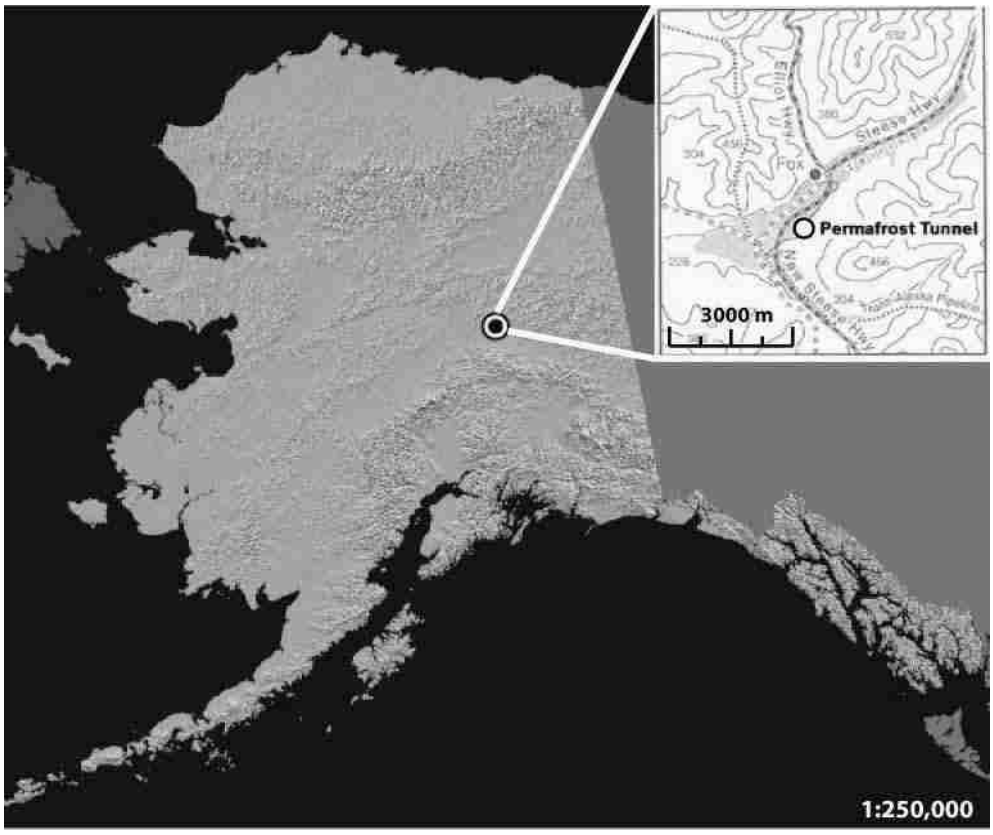

Figure 2. Location of CRREL permafrost tunnel on shaded relief map of Alaska. Detailed inset shows tunnel location on contour map (modified from http://agdc.usgs.gov/data/usgs/erosafo/300m/300m.html and http://permafrosttunnel.crrel.usace.army.mil/overview/location.html).

There is poor to fair stratification in the silt units, with stratification emphasized when ice seams and lenses are present (Pewe, 1975). Each silt unit contains its own generation of ice wedges, with the oldest wedges yielding radiocarbon ages of approximately 32 ka (Hamilton et al., 1998). Katayama et al. (2007) provided a radiocarbon age of 24,884 ± 139 years (29,824 calibrated years BP) from a methane sample collected from the ice

wedge studied in this project, likely from the center of the wedge. Further, an ice wedge from within the Goldstream Formation at the nearby Vault Creek permafrost tunnel was dated to 34.4 ka (Meyer et al., 2008). In the CPT, the younger silt layer unconformably overlies the older silt layer, the contact of which can be identified by the truncated tops of ice wedges in the bottom silt layer, which likely melted during a warm period (Hamilton et al., 1998).

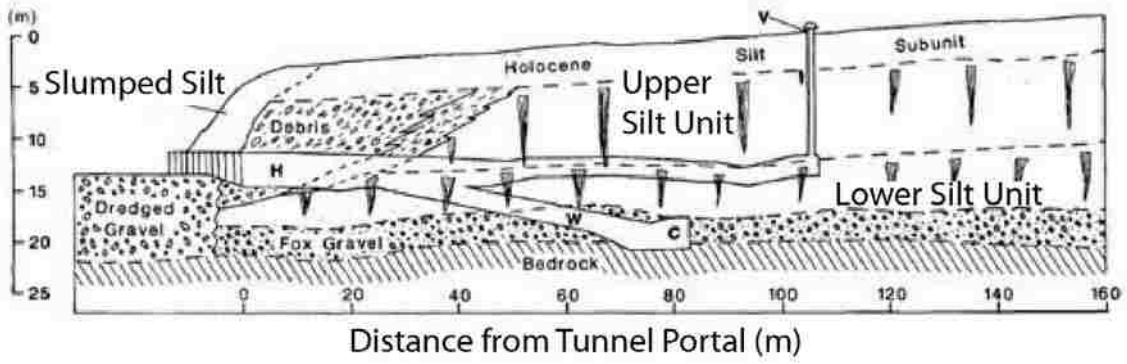

Figure 3. Tunnel cross section, showing horizontal adit (H) and declining winze (W), along with stratigraphy. Ice wedges are not necessarily located where drawn (modified from Hamilton et al., 1988).

Past Climate

Mapping and cosmogenic exposure dating of moraines, combined with analysis of loess and lake sediments has allowed for determination of a climate history of Alaska. Because of the diversity of Alaskan climate and elevation, heterogeneity exists in climate proxy records (Shulski and Wendler, 2007). However, global climate events can be correlated between records.

As most of Central Alaska was not glaciated during the large ice sheet advances throughout the Pleistocene (Kaufman et al., 2004), much land was not scoured by the ice

masses. This permitted some longer-term paleoclimate records to develop and persist through climatic ameliorations and degradations through time. The last interglaciation (~125 ka) is well documented in the Yukon-Tanana Uplands by the Eva Interglaciation Forest Bed, a perennially frozen forest encased in loess that is analogous to the modern boreal forest (Pewe et al., 1997), and is one of the older climatic events preserved in permafrost in Central Alaska.

Changes in magnetic susceptibility and grain size of loess reflect variations in wind intensity. Larger grains and increased magnetite are associated with the stronger winds of glacial intervals, and smaller grains and decreased magnetite with the weaker winds of interstadials (Beget, 1996). Magnetic susceptibility studies from Goldstream Formation loess deposits both in the CPT and elsewhere in the Fairbanks region were interpreted to reflect a period of climate amelioration from approximately 38 – 30 ka (Beget, 1990). Higher magnetic susceptibility levels from the same sections are interpreted to indicate higher wind intensity from 25-10 ka, in concert with permafrost aggradation and cool temperatures (Beget, 1990). Rapid changes between high and low susceptibility are also recorded in Fairbanks area loess, and Beget (1990) correlate a low susceptibility horizon to the melting of large ice wedges within the CPT.

During the late Pleistocene, glaciers in the Alaska Range expanded due to lower temperatures onto currently unglaciated lowlands, producing moraines and other glacial geomorphologic features recording their activity. The Cordilleran Ice Sheet of the last glacial maximum (~21 ka) extended west to the Aleutian Islands and north to the Alaska Range, and ice caps developed in the Brooks Range, culminating in a maximum total of 1,200,000 km^2 of Alaska once covered by glaciers (Kaufman et al., 2004). Late

Pleistocene pollen spectra from lakes across the region indicate a change from boreal forest to steppe or tundra vegetation common in dry and cool climates (Anderson et al., 2004). From studies of glacier fluctuations throughout the region, the most recent glaciation in the Alaska Range has been placed between 24,000 and 11,500 years ago, which is consistent with other global records of the late Wisconsin glaciation (Kaufman et al., 2004). Some portions of the Yukon-Tanana Upland were glaciated during Pleistocene advances by smaller valley glaciers, as at Mount Harper and the Ramshorn Creek valley, evidenced by mapping and cosmogenic exposure dating of morainal landforms (Briner et al., 2005; Weber, 1986). Lower elevation areas, including the present locations of Fairbanks and Fox, were unglaciated during this time.

As temperatures decreased during the glacial period, permafrost was able to develop due to unhindered interaction between the ground surface and cold air. There was a gradual return to modern boreal forest vegetation in the Holocene, with the expansion of white and black spruce (Anderson and Brubaker, 1994). Holocene glacial advances are recorded in mountain ranges across central Alaska, in particular during the Little Ice Age (1400 – 1900) (Calkin, 1988; Wiles et al., 2002). Since that time, there has been an overall climatic warming in Central Alaska, with a general retreat of glaciers and decrease in continuous permafrost at lower latitudes.

Modern Climate

Climate in Alaska is controlled by factors such as latitude, topography, and proximity to the ocean. The Fairbanks area and surrounding central Alaska has a subarctic continental climate (Hamilton et al., 1988; Hare and Hay, 1974). Continental climates are

characterized by long winters with extremely low temperatures and short summers with high temperatures (French, 2007). These large seasonal variations in temperature are due to differences in incoming solar radiation throughout the year at high latitudes. Incoming solar radiation in central Alaska is minimal during the winter. The 1961-1990 mean annual air temperature at Fairbanks was –2.8°C, and the mean July temperature was 16.9°C (Hare and Hay, 1974; Muhs et al., 2001). The Fairbanks average high temperature in July is 23°C, the average low in January is -28°C, and average annual snowfall is 173 cm (Shulski and Wendler, 2007). The 1961-1990 mean annual precipitation total at Fairbanks was 276 mm, and snow is generally present from October through April, with maximum snowfall occurring between October and January (Hamilton et al., 1988; Muhs et al., 2001).

The main circulation controls affecting Alaskan winter climate are the Siberian High, the Pacific subtropical high located over the Eastern Pacific Ocean and the Aleutian Low near the Aleutian Islands in the North Pacific Ocean (Mock et al., 1998). Decadal variability of the strength of the Aleutian Low has been observed and linked to the Pacific North American oscillation, with lower pressures associated with El Niño-Southern Oscillation and higher pressures during La Niña (Overland et al., 1999; Shulski and Wendler, 2007). Central Alaska generally experiences high pressure during the winter, with snowfall associated with low pressure systems. Circulation during winter months can be controlled by large-scale advection of warm air from the coastal south to the cold interior, resulting in significant increases of temperature to above-freezing conditions, known as chinooks (Shulski and Wendler, 2007).

Autumn freeze-up, when the mean daily air temperature falls at or below 0°C, takes place around 15 October in Central Alaska, occurring one month earlier in the extreme northern part of the state and a month later in the southern (Hare and Hay, 1974). By contrast, spring break-up, when mean daily air temperature rises to or above 0°C, occurs around 25 April in Fairbanks, around 1 April in the southern part of the state, and 1 June north of the Brooks range (Hare and Hay, 1974). Summer climate is largely affected by the Pacific subtropical high, as well as the polar front. The East Asian Trough in the 500 hPa geopotential height (pressure level approximately 5000 m from the ground), located through the Beaufort and Bering Seas, also has an affect on summer climate, creating southwest atmospheric flow over the state (Mock et al., 1998). In Central Alaska, there are frequent periods of rain during summer months due to cyclonic systems originating in Siberia or the Arctic Ocean, with thunderstorms common between May and August (Hare and Hay, 1974).

The ocean provides a moderating effect in coastal regions and a source of moisture to interior locations. Most precipitation in Central Alaska occurs during summer, produced primarily from the inland movement of Pacific storms and partially from weak cyclones moving from Siberia or the Arctic Ocean along the Arctic front (Hare and Hay, 1974; Muhs et al., 2001). There is a barrier effect of the mountain ranges to the south, including the Kenai, Chugach, Wrangell, Talkeetna and Alaska ranges, causing Pacific air masses to lose much of their moisture shortly after leaving the coast, often hindering their northward movement and contributing to extensive precipitation and glaciation in the south (Hare and Hay, 1974).

Permafrost

Permafrost is found across Alaska, in continuous, discontinuous, sporadic and isolated forms (Ferrians, 1998). The CPT is located in the zone of discontinuous permafrost, with average permafrost thicknesses of 30-120 m, and is north of the -1°C mean annual air temperature isotherm (French, 2007; Hamilton et al., 1988). Distribution of discontinuous permafrost in the vicinity of the CPT is controlled by factors such as slope angle, vegetation, snow cover, and presence of water bodies (French, 2007; Hamilton et al., 1988). The perennially frozen silt unit exposed within the CPT contains various forms of ground ice, including segregated as well as massive ice, the latter of which offer a unique opportunity to investigate past climatic events.

Ice wedges are a type of massive ground vein ice, in which repeated thermal-contraction cracks open at approximately the same location for a period of time, with snowmelt entering the open cracks and freezing, creating a wedge of foliated ice (Figure 4) (French, 2007). For thermal contraction cracking to occur, air temperatures are generally between -25°C and -40°C, the temperature at the top of the permafrost is usually between -10°C and -20°C, and the ground cooling rate between +0.1°C and -0.6°C/day (French, 2007). Epigenetic ice wedges form in pre-existing permafrost, and are younger than the surrounding sediments, with little sediment accumulating on the ground surface (Mackay, 1992). As epigenetic ice wedges form, a thermal-contraction crack opens to approximately the same depth at the same approximate location each time, growing wider but not taller, with the oldest ice toward the edges and youngest ice at the middle (French, 2007). Syngenetic ice wedges form in a similar manner, but grow mostly during, rather than after sediment deposition, increasing in height as the surface aggrades,

and ice is often similar in age to surrounding sediments (French, 2007). Field observations of modern ice wedge cracking by Mackay (1992) on Garry Island in the Arctic Coastal Plain indicated that cracking is most likely to occur toward the middle of an ice wedge, but can occur anywhere within the width of the ice. Cracking frequencies for ice wedges vary widely, loosely depending upon factors such as winter air temperatures, presence of vegetation, and depth of snow, but active ice wedges can crack once every 1 to 50 years (Mackay, 1992).

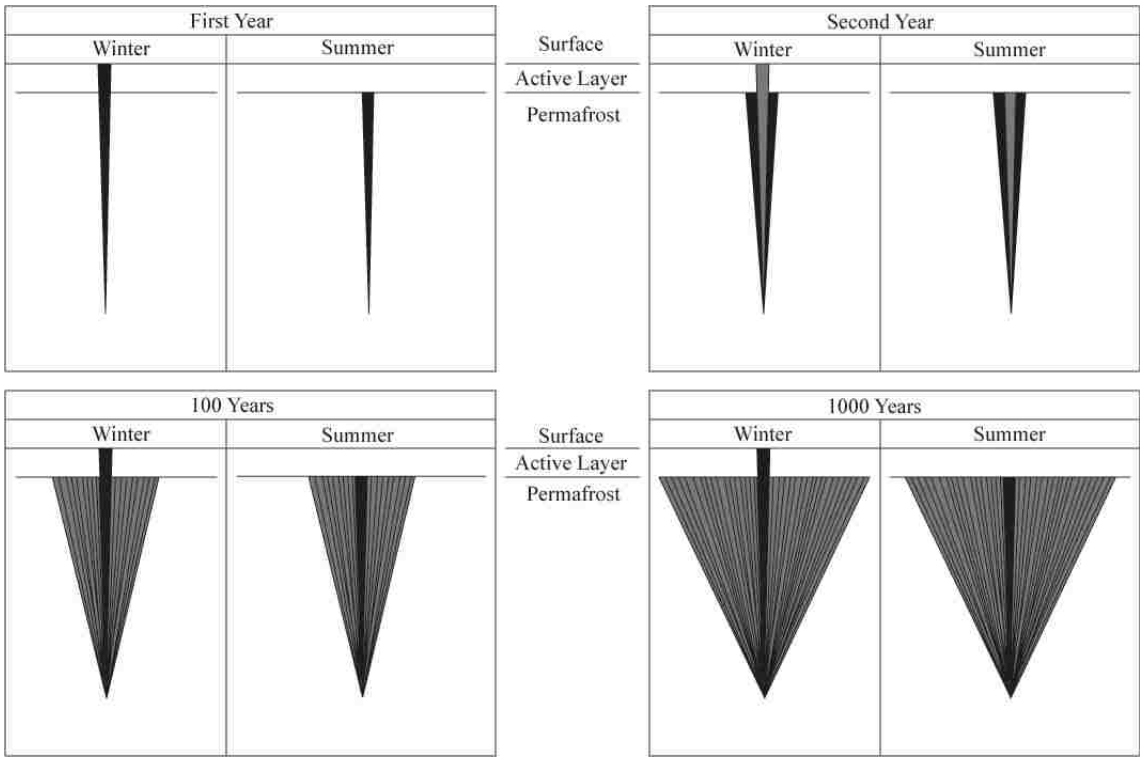

Figure 4. Diagram of ice wedge formation. In the first year, the ground contracts until it cracks from cold temperatures during the winter, and during the summer thaw melt water infiltrates and freezes within the crack. The second year, the ground cracks through the existing ice due to the plane of weakness, water infiltrates and freezes during thaw, and the ice wedge is made larger. Over time, as long as air temperatures are cold enough to crack the ground, the wedge continues to grow. Ice wedge and crack sizes are not to scale (modified from http://permafrosttunnel.crrel.usace.army.mil/permafrost/massive_ice.html).

With the onset of spring, cracks which can initially average 1-2 cm in width and 2.5–4 m in depth often decrease to 0.5-1 mm in thickness (Harry and Gozdzik, 1988). In order for active wedges to grow in size, thermal contraction cracks must remain open in order for meltwater to infiltrate and freeze. The meltwater that enters the crack is sourced from snow accumulated during the colder months, which upon freezing preserves information about winter precipitation.

Stable Isotopes and Radiocarbon Dating

Past winter air temperatures can be inferred from analyses of the stable oxygen isotope records in ground ice, such as from foliations in ice wedges. Isotopes are atoms with identical atomic numbers but different mass numbers due to different numbers of neutrons. Because of the difference in mass, ratios of heavier and lighter isotopes in water can change under different conditions, such as a change in phase or chemical transformations (Clark and Fritz, 1997). This fractionation of isotopes is due to differences in bond strength, so that heavy isotopes are preferentially partitioned into stronger bonds and favor a more condensed state because more energy is required to break those bonds. Therefore, during evaporation, water is more enriched in ^{18}O and vapor in ^{16}O.

Changes in $\delta^{18}O$ values of precipitation can occur as a result of Rayleigh distillation, in which equilibrium fractionation occurs during the phase change from vapor to condensate, increasingly depleting the air mass of the heavy isotope as it moves along a trajectory (Clark and Fritz, 1997; Sharp, 2007) (Figure 5). As the air mass becomes increasingly depleted in ^{18}O, each subsequent rain event becomes correspondingly depleted with respect to the remaining vapor from an earlier rain as isotopically heavy

water is continuously removed from the system. As the removal of moisture from an air mass causes variations in the isotopic composition of precipitation, various factors can affect the stable isotope values. For example, $\delta^{18}O$ values generally decrease with increasing latitude due to rain-out, as vapor is transported toward the poles from sources in the tropical oceans (Rozanski et al., 1993).

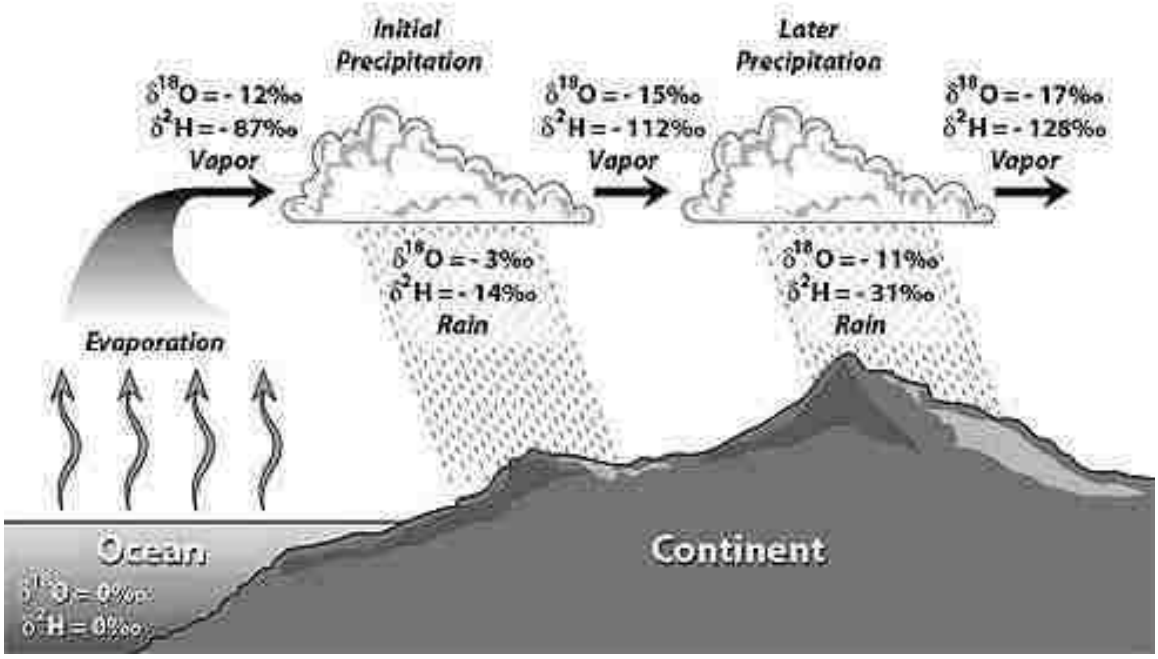

Figure 5. Change in the $\delta^{18}O$ and δD values of cloud vapor and rainfall due to Rayleigh distillation (Hoefs, 1997).

Air temperature can have an effect on stable isotope values as well, as cooling temperatures often result in condensation, and thus depletion of heavier isotopes (Dansgaard, 1964; Rozanski et al., 1993). Increased continentality leads to a larger seasonal cycle in stable isotopes, with a higher amplitude of the change in $\delta^{18}O$ seen between summer and winter (Rozanski et al., 1993). Isotope ratios of $^{18}O/^{16}O$ or $^{2}H/^{1}H$

relative to that of Standard Mean Ocean Water (SMOW) in the water molecules of the precipitation reflect the temperature of cloud vapor at the time of snow formation, and therefore the air temperature (Dansgaard, 1964). These are important values for determination of temperature information, with a more negative value indicating colder temperatures, and a more positive value indicating warmer temperatures.

While condensation is an equilibrium process, kinetic processes such as evaporation can also cause variation in $\delta^{18}O$ values. Evaporation at the snow surface causes kinetic isotopic enrichment due to isotopic exchange between vapor and snow (Clark and Fritz, 1997). Because the snowmelt process takes place at the snow surface, isotopic values can be affected by the isotopic exchange and redistribution that occurs between liquid water and ice as the water with higher $\delta^{18}O$ values percolates throughout the snowpack, with the $\delta D - \delta^{18}O$ slope value decreasing over time as $\delta^{18}O$ and δD values increase (e.g. Lee et al., 2010; Taylor et al., 2001). These variations, which occur as fresh snow evolves into snowmelt, are equilibrium processes. Although changes in isotopic composition do occur, there is not a significant difference between mean isotopic values of new snow and its eventual melt water, and average winter surface air temperatures are highly correlated to $\delta^{18}O$ values in ground ice (Lee et al., 2010; Nikolayev and Mikhalev, 1995).

The deuterium excess value ($d = \delta D - 8 \times \delta^{18}O$) is indicative of conditions at the moisture source where precipitation reaching the sampling locality originated, such as sea surface temperature and relative humidity (Clark and Fritz, 1997; Jouzel et al., 2007). Modern deuterium excess has an average value of 10‰, but varies regionally depending on local conditions. It is the differences in vapor pressures of the heavier water isotopes $^{2}H^{1}H^{16}O$ (HDO) and $H_2{}^{18}O$ that cause variations in deuterium enrichments in water

during evaporation (Clark and Fritz, 1997). During evaporation of sea water, there is a kinetic effect due to differences in the molecular diffusivities of HDO and $H_2{}^{18}O$, with deuterium excess values increasing with decreasing relative humidity. The diffusion of the different isotopes into the air column is largely dependent upon relative humidity at the source. When there is low humidity, there is more diffusion of water molecules during kinetic evaporation from the ocean into the atmosphere than from the atmosphere into the ocean, and the resulting vapor is more depleted in heavier isotopes than lighter.

Precipitation in the high latitudes has a strong seasonal signal, with $\delta^{18}O$ of precipitation varying along with the high seasonal variations in temperature (Rozanski et al, 1993). This signal is seen in $\delta^{18}O$ measurements in Fairbanks (Yoshikawa and Hinzman, 2003). Due to the large changes in temperature between summer and winter associated with the continental climate, the $\delta^{18}O$ values of precipitation in Fairbanks range from approximately -37‰ to -5‰, with snowmelt water values of around -23‰ (Yoshikawa and Hinzman, 2003). A local meteoric water line (LMWL) is useful in determining the ratio of δD to $\delta^{18}O$, represented the slope of the line, with the intercept demonstrating the amount of kinetic fractionation from evaporation, reflecting differences in temperature and relative humidity. The Fairbanks LMWL is defined as $\delta D = 6.7 \times \delta^{18}O - 21.589$ (Yoshikawa and Hinzman, 2003).

The global stable isotopic composition of modern precipitation in the high latitudes is understood through analysis of data from the International Atomic Energy Agency's (IAEA) Global Network of Isotopes in Precipitation (GNIP) (e.g., Rozanski et al., 1993), which provide $\delta^{18}O$ and δD information for multiple locations. While the few GNIP stations in Alaska and nearby territories are too widely spaced for a detailed study of

local stable isotope variations, there are enough stations to provide a general understanding of modern isotopic values in continental locations at high latitudes. GNIP stations in Alaska are located in Barrow on the far northern Arctic coast, Adak in the Aleutian Islands, Bethel in the southwestern peninsula, and Inuvik on the Mackenzie River Delta near the Arctic Coast of the Northwest Territories. Nearby GNIP stations with similar climatic controls as Fairbanks are located in Mayo and Whitehorse in the Yukon Territory, and Yellowknife in the Northwest Territories (Figure 6).

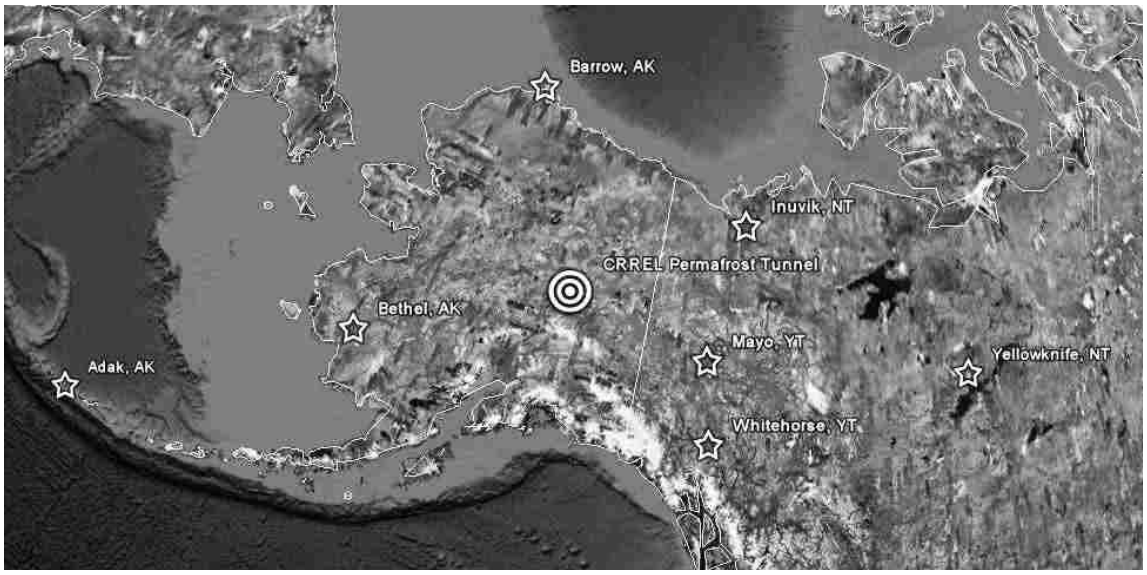

Figure 6. Google Earth image of Global Network of Isotopes in Precipitation station locations in relation to the CRREL Permafrost Tunnel.

From the GNIP data, both spatial relationships between long-term averages of isotopes in precipitation and surface air temperature, and temporal relationships between seasonal changes of isotopes in precipitation and temperature can be determined. Temperature gradients provide the relationship between $\delta^{18}O$ in precipitation and surface air temperature, with the slope of this relationship describing the change in temperature

associated with each ‰ change in $\delta^{18}O$ (Rozanski et al., 1993). The slope of this relationship has been defined globally as 0.69‰ per °C for $\delta^{18}O$ and 5.6‰ per °C for δD (Dansgaard, 1964). Local temporal and spatial isotope gradients will be discussed below.

While stable isotopes are important for determination of temperature of condensation, radiocarbon dating is important for establishing the timing of temperature anomalies. The radioactive isotope carbon-14 (^{14}C) is formed in the atmosphere, when neutrons produced by cosmic rays interact with ^{14}N according to the formula

$$^{14}N + n \rightarrow {}^{14}C + p$$

and decays as follows

$$^{14}C \rightarrow {}^{14}N + \beta^-$$

with a half-life of 5730 years (Olsson, 1991). Relative to the percentage of all carbon, ^{14}C has the very low abundance of 10^{-10}% compared to the two stable carbon isotopes, ^{12}C (98.9%) and ^{13}C (1.1%) (Olsson, 1991). ^{14}C is incorporated into all living plants and animals, as it is oxidized to carbon dioxide, and begins to decay with time after the organisms die. The radiocarbon dating method measures the amount of ^{14}C remaining in an organic sample, so that the amount of time since its death can be established.

CHAPTER 3

METHODS

Sampling Technique

I selected an ice wedge 50 m from the tunnel portal on the south wall of the main adit for $\delta^{18}O$ and δD analysis based on optimal exposure and accessibility (wedge 50S) (Figure 7). The wedge is located within the Goldstream Formation, encased mostly in bedded silt and massive silt with rootlets and organic matter. The top of the wedge is truncated, and overlying sediments contain patches of organic matter, as well as horizontal elongated lenses of clear ice adjacent to reticulated ice. Hamilton et al. (1998) interpreted the clear ice lenses seen throughout the CPT as buried surface thaw ponds, or "pond" ice. The clear massive ice bodies have since been interpreted as "cave" ice, which is the result of preferential melt-erosion along ice wedge polygons (Bray et al., 2006; Shur et al., 2004). A thin 3.6 cm wide vein of foliated wedge ice penetrates the sediments above 50S, extending from the ceiling of the tunnel and penetrating the top of the right half of the wedge. A folia traced from the thin vein intersects the isotope sampling transect at 111.5 cm from the left.

The exposure of wedge 50S had a near-vertical face with minimal disturbance and folia in the ice wedge were nearly perpendicular to the exposure. Along the exposed face, the wedge is 246 cm wide along the top, and 105 cm tall in the center. Many foliations within the ice wedge contain fine sediment, and particularly silt-rich foliations are located at 27.8 cm, 49.0 cm, 68.0 cm, and between 82-97 cm. A 126 cm long rectangular slab cut along the entire width of the ice wedge near the bottom was sub-sampled in a cold laboratory at the CRREL facilities at Fort Wainwright Army Post at approximately $-7^{o}C$.

I cut sub-samples approximately 2 mL in volume along the length of the slab approximately parallel to the dominant folia orientation at 5-10 mm intervals using a coping saw (Figure 8). The first 15 samples were 5 mm wide, after which I increased the sampling width to 10 mm to ensure a large enough volume of ice to fill the 2 ml sample vials for isotope analysis, yielding a total of 135 samples, each containing 1-4 apparent folia. Individual folia were distinguishable by clear bubbly ice bounded on either side by darker sediment rich ice. To prepare for stable isotope analysis, I removed sediment in the melted ice using a polypropylene filter with a 0.2 μm membrane affixed to a syringe, and transferred to 2 mL glass vials. Oxygen and hydrogen isotope analysis of samples collected from 50S, as well as surface water samples collected in the Fairbanks region and near the Wulik River in northwest Alaska, was performed at the Las Vegas Isotope Science Laboratory (LVIS) at the University of Nevada, Las Vegas.

In order to test if more variation in oxygen and hydrogen isotope values could be detected by including fewer folia in each individual sample, I collected additional samples for stable isotopes at a higher resolution sampling interval of 2 mm for a 10 cm wide section of the slab. A device (Figure 9) for high-resolution ice subsampling was designed, consisting of a high speed rotary tool, a drywall square, and two chemistry lab ring stands. The chemistry stands were set at either end of the drywall square, with the square clamped to the stands allowing for vertical adjustment. The sliding arm of the square had a guide bored through it to allow the cutting head of the high speed rotary tool to cut specific increments from the ice. Ice was milled to a depth of 16 mm from the surface at 2 mm wide intervals. I then filtered the samples and placed them in glass vials in the same method as previously described. Fifty total samples were collected from 12.5

Figure 7. Image of wedge 50S after sampling, with interpretive sign for scale. “Cave” or “pond” ice, as well as wedge 50S and the thin wedge ice are indicated with arrows. The rectangular recess is the location of the sampled wedge ice for this study.

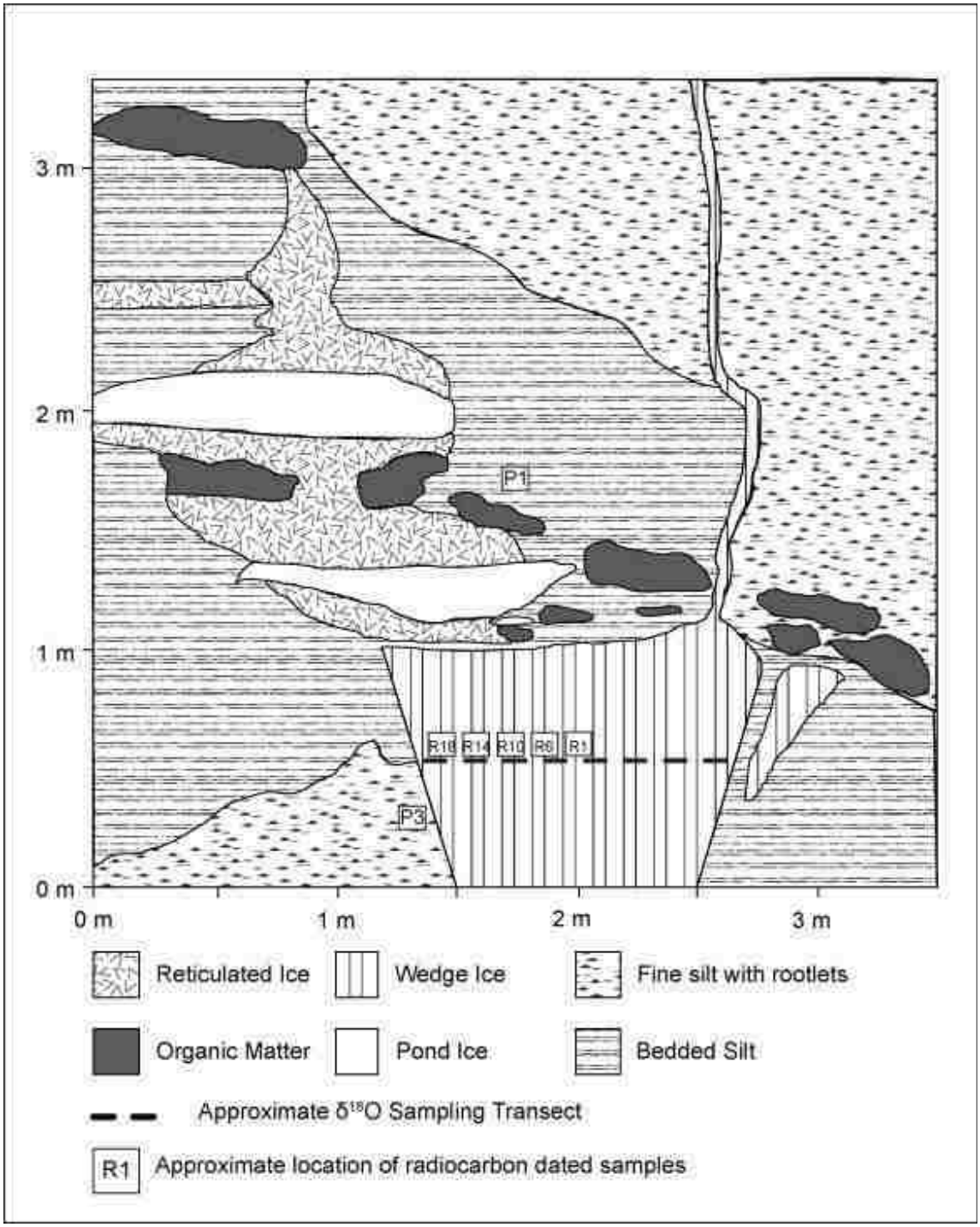

Figure 8. Schematic of wedge 50S, sampled 50 m from portal on south wall of main adit. Dashed line indicates approximate location of $\delta^{18}O$ sampling transect. Approximate locations of radiocarbon dated samples from within the wedge (R1, R6, R10, R14, and R18) and from outside the wedge (P1, P3) indicated by labeled boxes.

Figure 9. High-resolution isotope sampling device, with partially sampled ice block.

Oxygen and Hydrogen Isotope Analysis

to 22.5 cm from the left edge of the wedge and sent to the Saskatchewan Isotope Laboratory at the University of Saskatchewan for stable isotope analysis.

Water samples obtained from the ice wedge were analyzed for $\delta^{18}O$ and δD using a ThermoElectron high-temperature Thermal Conversion Elemental Analyzer (TC/EA) coupled to a ThermoElectron Delta V Plus Stable Isotope Ratio Mass Spectrometer in continuous flow mode at the University of Nevada, Las Vegas, Las Vegas Isotope

Science Laboratory (LVIS), following the procedure of Sharp et al. (2001). The TC/EA converts the water samples into the gases CO and H_2, as products of the reduction reaction:

$$H_2O + C \rightarrow H_2 + CO$$

when run through a ceramic reduction column lined with a coarse glassy carbon-packed glassy carbon sleeve at 1450°C while entrained in a helium carrier gas (Sharp et al., 2001). The H_2 and CO are separated in a gas chromatographic column and then directed via the ConFlo III interface to the isotope ratio mass spectrometer where the ratio of heavy to light isotopes of the CO and H_2 gases, $^{18}O/^{16}O$ and $^{2}H/^{1}H$, are measured. These ratios are expressed as parts per thousand (‰) deviation relative to a standard, which is defined as:

$$\delta = \left(\frac{R_{sample}}{R_{s\tan dard}} - 1 \right) \times 1000$$

where R_{sample} is the $^{2}H/^{1}H$ or $^{18}O/^{16}O$ ratio of the sample, and $R_{standard}$ is the same ratio of the standard (Rozanski et al., 1993).

I performed a variety of statistical and graphical analyses on measured $\delta^{18}O$ and δD values from wedge 50S. To observe variations in $\delta^{18}O$ with time, I plotted the isotopic value of each sample with distance from the left edge of the wedge, assuming that age increases from the middle outward in a semi-symmetrical fashion. The relationship between δD and $\delta^{18}O$ was plotted and calculated in order to obtain information about the source, and for comparison against modern meteoric water lines. For comparison, I plotted δD and $\delta^{18}O$ values from 50S along with unpublished isotopic compositions of modern winter precipitation (Douglass, 2010).

Radiocarbon Dating

After collecting water samples, I sub-sampled the wedge for organic carbon for radiocarbon dating. Hydrogen peroxide was added to a few selected filtered sediment samples to confirm the presence of organic matter, by effervescence, for radiocarbon dating. I collected five initial samples for radiocarbon dating from sediment filtered from the same split as the stable isotope subsamples. The radiocarbon subsamples were selected at approximately 10 cm intervals from the left side of the wedge and submitted to Beta Analytic for radiocarbon analysis. In order to obtain and preserve the 500 μg of carbon, the sediment was pretreated at Beta Analytic with a light acid and no alkali.

A second batch of radiocarbon subsamples were separated from approximately 10 mm wide slabs of ice. These samples were cut using a box saw along the dip of the folia. The precautions I took to avoid contamination of the organic samples included wearing full-body Tyvek coveralls when sampling, and cleaning the box saw between each cut. Further, I shaved off the outer surface of each block with a chisel before cutting samples to minimize surface contamination with organic material derived from other sources. The sampling surface was covered by plastic sheeting, which was changed in between the extraction of each sample. I took these precautions for every organic sample to reduce the possibility of the inclusion of any carbon outside of each collected section of ice.

Cutting along rather than across folia minimized the number of folia contained within each sample. I cut ten samples from the middle of the wedge, visually estimated at 61.3 cm from the left margin. Samples were then cut at each 5 cm interval from the middle to either edge of the slab. While the sample cuts were 10 mm apart, the final width of each slab was approximately 8 mm due to the width of the saw blade and ice lost during the

cutting process. Forty six total samples were acquired, which were allowed to melt at room temperature before collection in 0.5 L Nalgene bottles. I washed sediments remaining at the bottom of the sample collection containers into the bottles using a funnel with filtered and distilled water. The five samples selected for these radiocarbon ages (Samples 50S-09-R1, R6, R14, R18) (Figure 8) are from similar locations as the first radiocarbon samples, providing an opportunity to verify or replace those initial dates. In order to assist in constraining the age of the wedge, I also collected two preserved and frozen rootlets or sticks (samples 50S-09-P1 and 50S-09-P3) from the frozen sediments to the left of and above the ice wedge for standard AMS dating (Figure 8). I used IntCal 09 to convert radiocarbon ages obtained from Beta Analytic to calibrated years BP (Reimer et al., 2009; Stuiver and Reimer, 1993).

GNIP Analyses

In order to better quantify the changes in temperature associated with measured variations in $\delta^{18}O$, I utilized stable isotope data from modern precipitation at GNIP stations in and near Alaska at Adak, Barrow, Bethel, Inuvik, NWT, Mayo, YT, Whitehorse, YT and Yellowknife, NT. Values for $\delta^{18}O$ and δD were also plotted against the GMWL to investigate conditions such as relative humidity and temperature at the moisture source. Average monthly precipitation and $\delta^{18}O$ values were plotted against time in order to gain an understanding of the relationship between those two variables.

To develop a temporal linear relationship between temperature and $\delta^{18}O$ for each station, I calculated linear regressions using mean monthly temperature and precipitation weighted $\delta^{18}O$ measurements from each GNIP site. The slope from this linear regression

provides the ‰ change in $\delta^{18}O$ per 1°C change in temperature. The coefficient of determination, or R^2 value, indicates the amount of variation in $\delta^{18}O$ explained by a 1°C change in temperature. A spatial relationship between $\delta^{18}O$ and temperature was also calculated by averaging the monthly mean $\delta^{18}O$ and air temperature values for each station, and performing a linear regression on those values. A linear regression was calculated using mean monthly values (n = 12) from all stations. Because ice wedge ice is sourced from snowmelt, I calculated linear regressions using only the mean monthly temperature and $\delta^{18}O$ values measured during winter months to examine the relationship in solid precipitation. Winter months were identified as October through March, when temperature is consistently below freezing.

CHAPTER 4

RESULTS

GNIP Analyses

Quantitative temperature estimates were made for the change in stable isotopes recorded in the ice wedge by employing local relationships between air temperature and $\delta^{18}O$ derived from GNIP data. Linear regressions of temperature and precipitation-weighted $\delta^{18}O$ values for each station are found in Table 1 and Figure 10. Figure 11A displays both the monthly temperature gradient and precipitation gradient for coastal stations, and 11B the gradients for continental stations. At Adak, changes in average monthly $\delta^{18}O$ values show no significant correlation with average monthly temperature (n=12), with an R^2 value of 0.01. There is a correlation between temperature and $\delta^{18}O$ in the other coastal stations of Inuvik, Barrow and Bethel, supported by R^2 values of 0.64, 0.69 and 0.78, respectively. The slope of the $\delta^{18}O$ – temperature line provides values of 0.08‰ per 1°C change for Adak, 0.29‰ per °C for Barrow, 0.19‰ per °C for Bethel, 0.49‰ at Inuvik, 0.26‰ per °C for Mayo, 0.21‰ per °C for Whitehorse, and 0.24‰ per °C for Yellowknife. The slope of the spatial $\delta^{18}O$ – temperature line using averaged values from all stations using all months supplies values of 0.73‰ per °C and 0.78‰ per °C for all stations during winter months, providing a spatial relationship between the two variables.

Table 1. Meteoric water line and T - $\delta^{18}O$ relationship for GNIP stations in Adak, Barrow, Bethel, Inuvik, Mayo, Whitehorse, and Yellowknife. MWL calculated using all values, T - $\delta^{18}O$ relationship calculated from mean monthly values (n=12).

GNIP Station	**MWL**	**T-$\delta^{18}O$ relationship**
Adak	$\delta D = 6.86(\delta^{18}O) - 3.26$ ($r^2 = 0.85$)	$\delta^{18}O = 0.02(T) - 8.96$ ($r^2 = 0.01$)
Barrow	$\delta D = 7.12(\delta^{18}O) - 9.13$ ($r^2 = 0.94$)	$\delta^{18}O = 0.26(T) - 15.29$ ($r^2 = 0.69$)
Bethel	$\delta D = 5.86(\delta^{18}O) - 25.21$ ($r^2 = 0.94$)	$\delta^{18}O = 0.18(T) - 12.3$ ($r^2 = 0.78$)
Inuvik	$\delta D = 7.33(\delta^{18}O) - 3.55$ ($r^2 = 0.98$)	$\delta^{18}O = 0.34(T) - 22.75$ (r2 = 0.64)
Mayo	$\delta D = 6.27(\delta^{18}O) - 36.86$ ($r^2 = 0.94$)	$\delta^{18}O = 0.28(T) - 21.60$ ($r^2 = 0.90$)
Whitehorse	$\delta D = 6.35(\delta^{18}O) - 30.58$ ($r^2 = 0.93$)	$\delta^{18}O = 0.17(T) - 21.61$ ($r^2 = 0.49$)
Yellowknife	$\delta D = 0.24(\delta^{18}O) - 20.55$ ($r^2 = 0.95$)	$\delta^{18}O = 0.22(T) - 20.48$ ($r^2 = 0.85$)

Stable Isotopes

Wedge 50S $\delta^{18}O$ values from the lower resolution 5 to 10 mm sampling intervals plot against distance from the left end with highest values toward the edges of the ice wedge and lowest toward the middle. These values range from a maximum value of -22.0‰ to a minimum value of -27.9‰, with a total difference of 5.95‰ (Figure 12). Basic descriptive statistics can be found in Table 2, where the mean $\delta^{18}O$ value is -26.3‰, the median value is -26.8, and standard deviation is 1.24. These values are similar to those seen in modern winter precipitation in the Fairbanks area (Figure 13, Table 2) (Douglass, 2010; Yoshikawa and Hinzman, 2003). Values of $\delta^{18}O$ from the high resolution sampling between 12.5 and 22.5 cm range from -26.7‰ to -24.8‰, with a mean value of -26.0‰ (Figure 12). Low resolution $\delta^{18}O$ values from that same interval range from -27.0‰ to -25.1‰, with a mean value of -26.3‰.

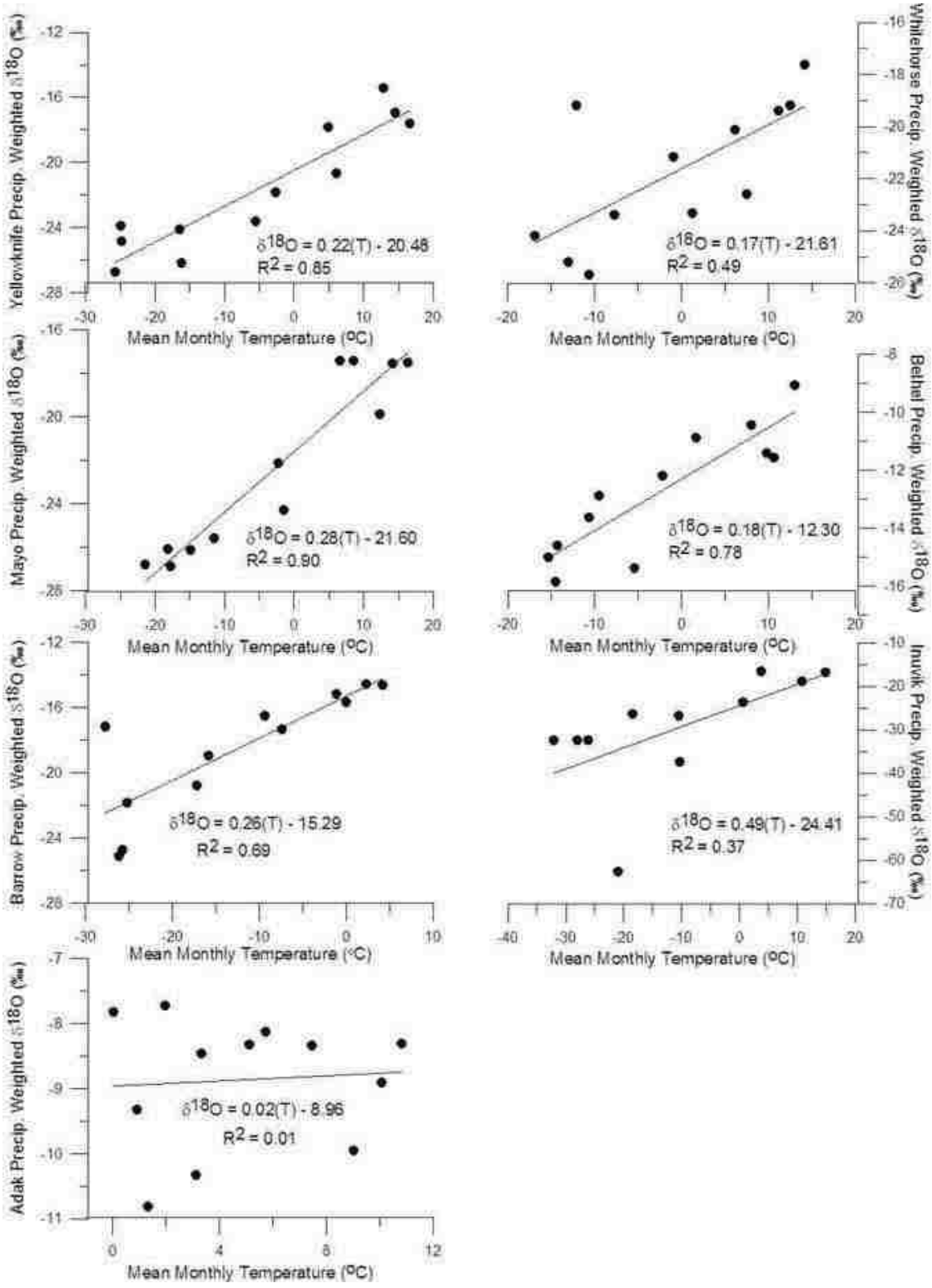

Figure 10. Precipitation weighted $\delta^{18}O$ linearly regressed against mean monthly temperature for GNIP stations at Yellowknife, Whitehorse, Mayo, Bethel, Barrow, Inuvik, and Adak. Slope of line represents the ‰ change in $\delta^{18}O$ for each 1°C change in temperature.

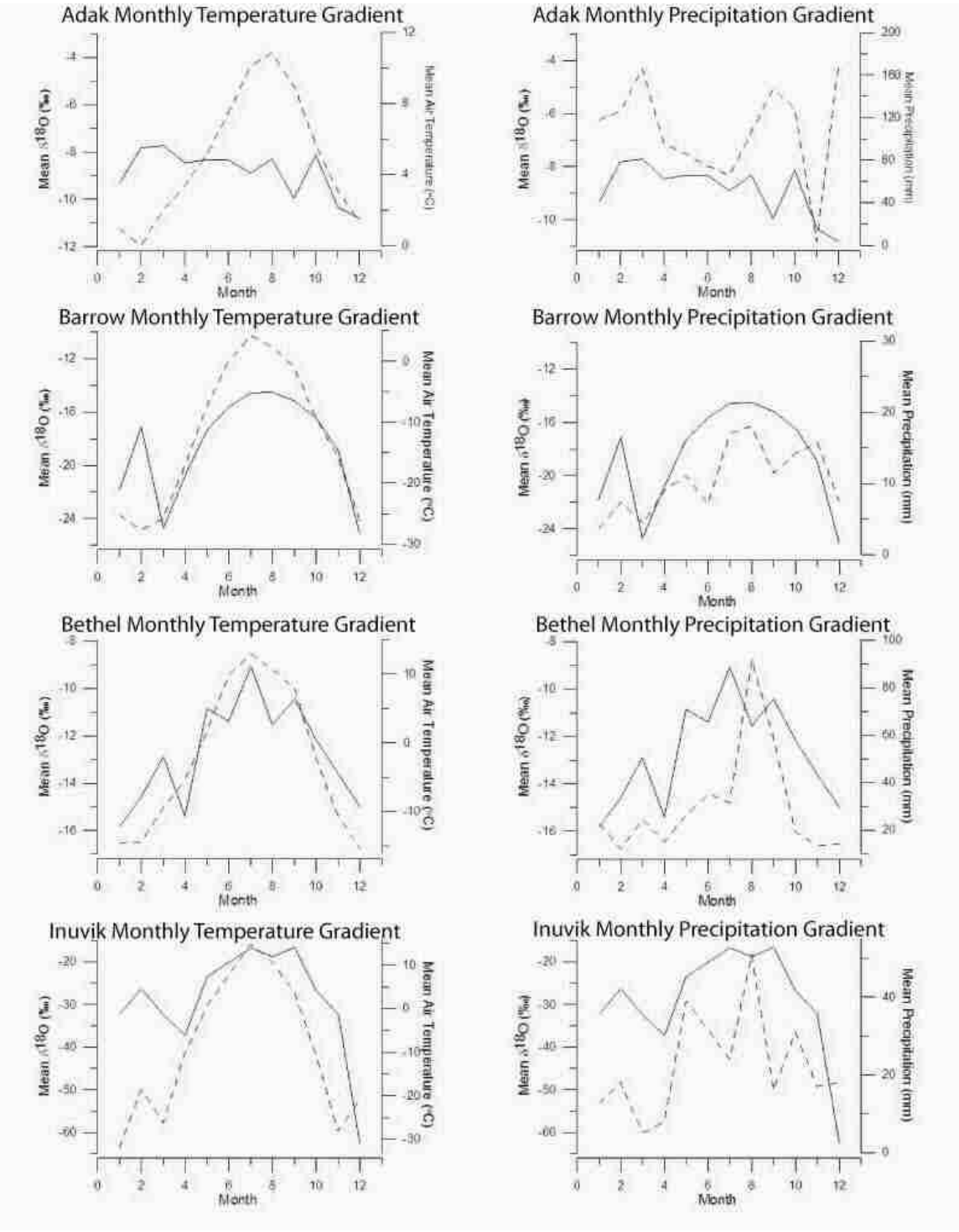

Figure 11-A. Temporal T – $\delta^{18}O$ and precipitation – $\delta^{18}O$ relationships for Adak, Barrow, Bethel, and Inuvik. The plots show the relationship between changes in $\delta^{18}O$ with changes in temperature and precipitation with time. Dashed line in the temperature gradient is mean air temperature, and represents mean precipitation in the precipitation gradients. In all figures, the solid line is mean $\delta^{18}O$.

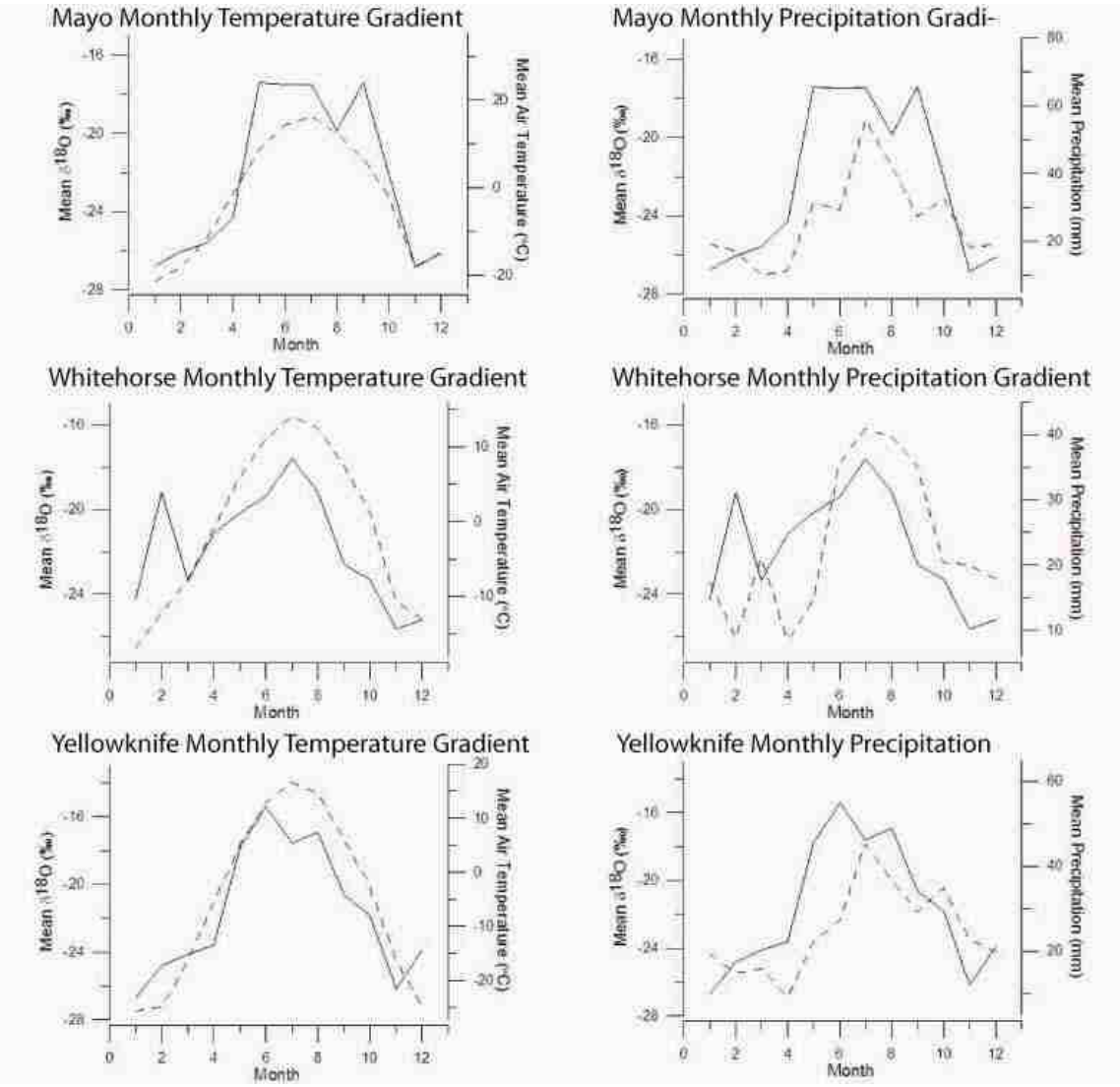

Figure 11-B. Temporal T – $\delta^{18}O$ and precipitation – $\delta^{18}O$ relationships for Mayo, Whitehorse, and Yellowknife. The plots show the relationship between changes in $\delta^{18}O$ with changes in temperature and precipitation with time. Dashed line in the temperature gradient is mean air temperature, and represents mean precipitation in the precipitation gradients. In all figures, the solid line is mean $\delta^{18}O$.

The leftmost edge of the wedge records the highest $\delta^{18}O$ value of -22.0 ‰, and the values gradually decrease to -26.3‰ at 14.5 cm (all distances are expressed in cm from the left). The $\delta^{18}O$ values continue to decrease to a value of -27.2 ‰ at 27.5 cm. Continuing across the wedge, the values remain fairly stable, with a few peaks less than

1‰, before decreasing to the minimum value of -27.9‰ at 90.5 cm. The $\delta^{18}O$ values then increase to -26.4‰ at 93.5 cm and continue to rise toward the right edge of the wedge, reaching a maximum of -24.4‰ at the right edge. Surface water samples collected in the Fairbanks region had $\delta^{18}O$ values ranging from -17.4‰ to -22.9 ‰. Northwestern Alaska surface water samples were similar, ranging from -16.84 to -21.29 (Figure 13).

Deuterium excess values from 50S slowly increase from about -0.3‰ at the left edge of the wedge to a maximum of 19.0 at 90.5 cm, before decreasing to 3.4‰ at 93.5 cm. The values then remain fairly steady to the right side of the wedge (Figure 14). A high concentration of thick, silt-rich folia was observed between 82 to 97 cm, straddling the location where the decrease in deuterium excess and the lowest $\delta^{18}O$ value were measured.

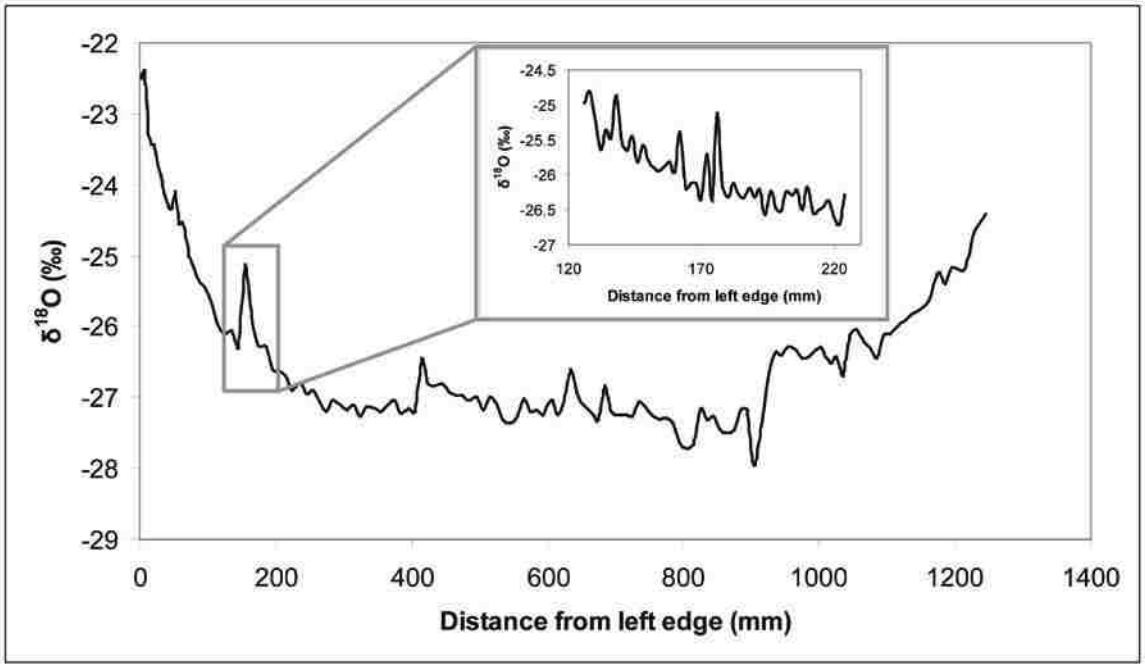

Figure 12. $\delta^{18}O$ values from wedge 50S with distance from the left edge of the wedge at 5 – 10 mm intervals. Inset contains $\delta^{18}O$ values from the high resolution re-sampling performed from 125-225 mm from the left, at 2mm intervals.

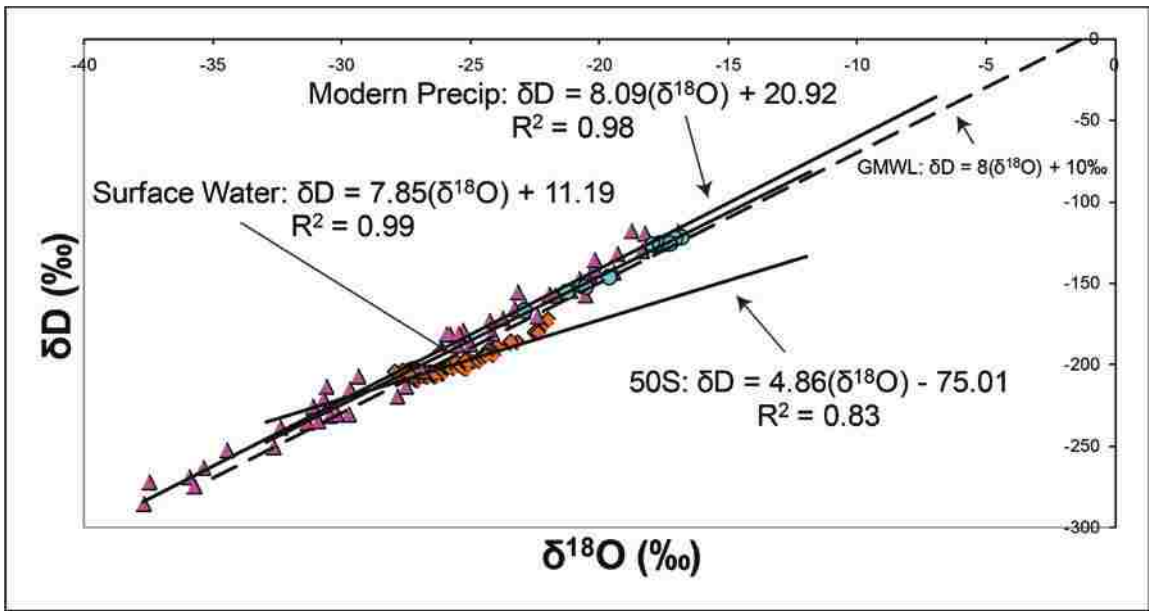

Figure 13. $\delta^{18}O$ and δD values and meteoric water line equations of modern winter precipitation in Fairbanks (purple triangles), modern surface water (blue circles), and ice in wedge 50S (orange diamonds), along with the global meteoric water line (dashed line).

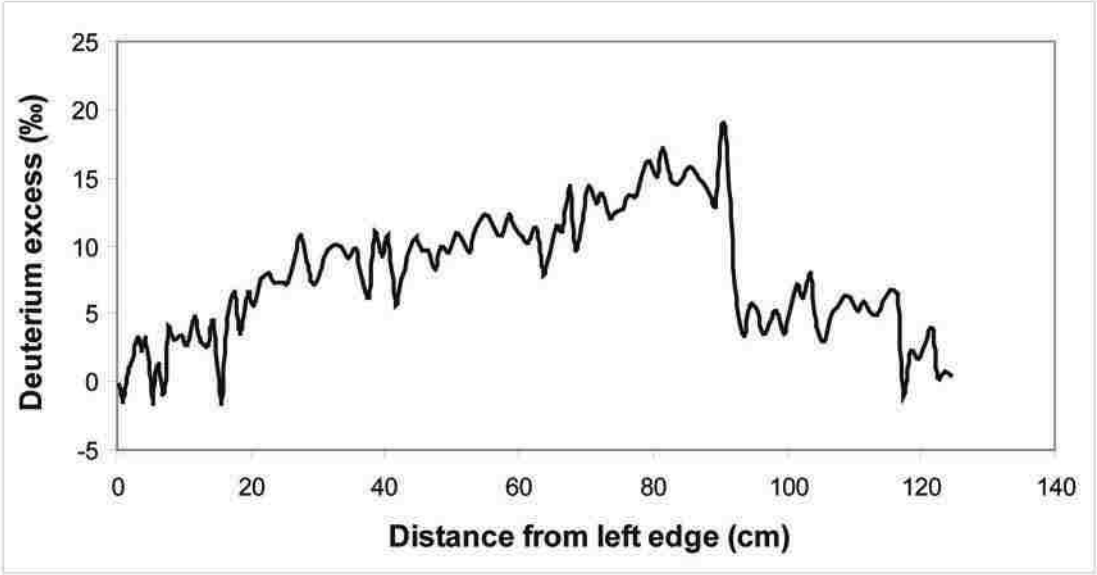

Figure 14. Deuterium excess values from wedge 50S with distance from the left edge of the wedge.

Table 2. Descriptive statistics of $\delta^{18}O$ values from 50S and modern winter precipitation in Fairbanks, AK.

Statistic	50S $\delta^{18}O$ (‰)	Modern Winter Precipitation $\delta^{18}O$ (‰)
Mean	-26.31	-26.31
Median	-26.81	-25.49
Min	-27.94	-37.69
Max	-21.99	-16.95
Range	5.95	20.74
Standard Deviation	1.24	5.68
n	135	48

Radiocarbon Dating

My initial attempt at radiocarbon dating was unsuccessful due to an insufficient amount of carbon in the organic samples. However, the second sampling effort with larger subsamples produced enough carbon for dating. The initial organic matter was filtered from 2 mL vials of melted wedge ice, while the second group of sediment was obtained from 0.25 to 0.75 mL of ice. I calibrated radiocarbon ages to calibrated years before present (cal yr BP) using IntCal 09 (Reimer et al., 2009). Calibrated ages of organic material contained in the folia of the ice vary considerably (Table 3). Organic material collected from 19.5 – 20.5 cm provide a calibrated age of 34,727 ± 142 years; from 29.5 – 30.5 cm the age is 36,991 ± 350 years, 35718 ± 246 years from 39.5 – 40.5 cm, and the age is 28,275 ± 182 years from 50.5 – 52.0 cm (Table 3). The center of the wedge was visually estimated at 61.3 cm, both by examining the wedge in the tunnel and the sampled slab in the cold laboratory, to determine where the folia were the most vertical. Sediments from that location provide a date of 32643 ± 369 years, approximately 4,820 years older than sediments 10 cm to the left from sample R6. The stick found in the frozen sediments to the left of the ice wedge provided a calibrated age of 40,837±374 years BP, older than any dates obtained from within the wedge. The stick

from sediments above the wedge gave a calibrated age of 34,765 ± 199 years BP, older than some of the sediments found within the wedge.

Table 3. Radiocarbon and calibrated ages of organic material from 50S. Samples 50S-09-R1, R6, R10, R14, and R18 were collected from within the foliated ice of the wedge. Sample50S-09-P1 was a stick found above the truncated top of the wedge, and sample 50S-09-P3 was a stick found in the sediments to the left of the wedge. Radiocarbon ages obtained from Beta Analytic were converted to calibrated years BP using IntCal 09.

Sample ID	Distance from left (cm)	Radiocarbon Age	Calibrated Age 1σ Range (yr cal BP)	Mean Calibrated Age (yr cal BP)
50S-09-R1	60.3-61.3	28330±180	32274-33012	32643
50S-09-R6	50.5-52.0	23510±130	28093-28456	28275
50S-09-R10	39.5-40.5	31470±230	35472-35963	35718
50S-09-R14	29.5-30.5	32540±270	36641-37340	36991
50S-09-R18	19.5-20.5	30060±210	34585-34869	34727
50S-09-P1	above wedge	30100±300	34566-34963	34765
50S-09-P3	left of wedge	35600±340	40463-41211	40837

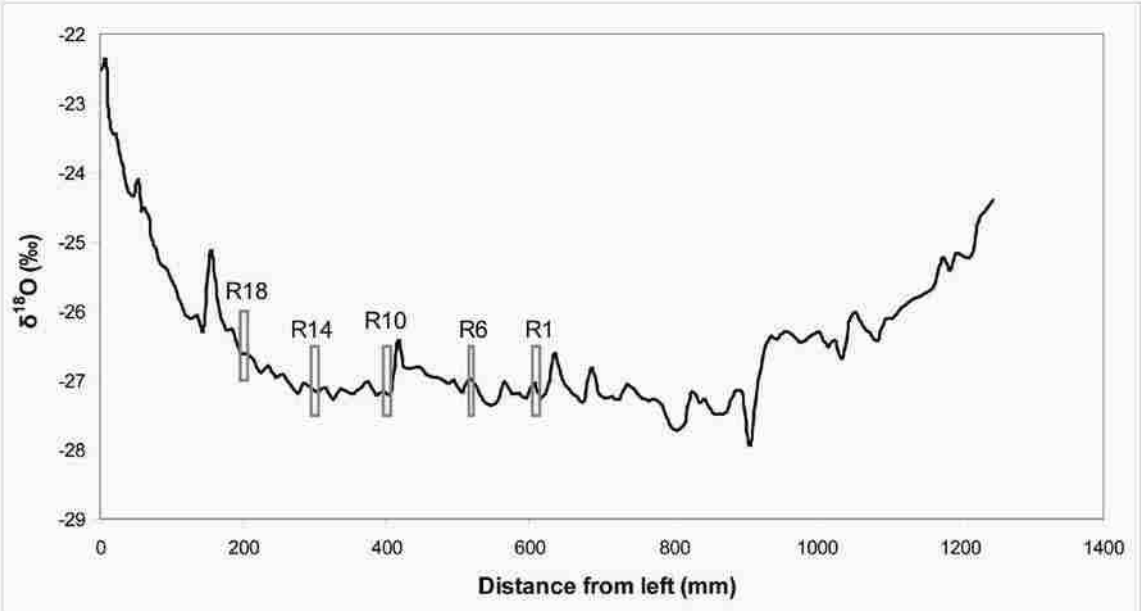

Figure 15. $\delta^{18}O$ values from 50S with distance from the left edge of the wedge. Labeled boxes represent true widths of radiocarbon dating sampling intervals: R1 (32.6 kyr BP), R6 (28.3 kyr BP), R10 (35.7 kyr BP), R14 (37.0 kyr BP), and R18 (34.7 kyr BP).

CHAPTER 5

INTERPRETATIONS AND DISCUSSION

I interpret the $\delta^{18}O$ values of wedge 50S to record a cooling event, as evidenced by a decrease in $\delta^{18}O$ values from -22‰ to -28‰ from the edges to the center of the ice wedge. $\delta^{18}O$ and δD values from 50S fall around the mean values of modern winter precipitation. The mean $\delta^{18}O$ value of -26.31‰ from 50S is precisely the same value measured in modern winter precipitation at Fairbanks, Alaska (T. Douglass, personal communication, 2010). Modern winter precipitation displays a higher range of values than I measured in wedge 50S. The smaller range measured in the ice wedge may be attributed to the homogenization of isotopic values experienced during the melting of seasonal snow cover, or due to sampling across folia.

I recognize four climatic conditions within the isotope series. First, a threshold condition was reached when temperatures became cool enough for thermal contraction cracking to begin; this condition occurred when $\delta^{18}O$ values of winter precipitation were about -22.0‰. Second, upon initiation of regular thermal contraction cracking, decreasing $\delta^{18}O$ values indicate a cooling event recorded in the first ~28 cm of ice wedge growth. The third condition is a relatively stable climate, during which time winter temperatures were cold enough for regular ice wedge growth, and $\delta^{18}O$ values of winter precipitation oscillated about a mean of -27.1‰; this stable interval is represented by the ice near the center of the wedge between 37.5 and 61.5 cm.

The fourth climatic condition is recorded in the center of the wedge, where a rise in $\delta^{18}O$ values is not recorded prior to the end of growth; rather, cracking stopped abruptly following an apparent stable cold period, suggesting a sudden rise in winter air

temperatures to levels above the range at which ice wedges form. Climatic amelioration is further signified by the truncation of the ice wedge, as evidenced by the blunt top overlain by a silt layer containing frozen thaw ponds or cave ice, associated with thermokarst erosion, as well as reticulate cryostructures indicative of permafrost thaw and refreeze (e.g. Shur et al., 2004).

In addition to evidence of permafrost thaw in sediments above wedge 50S, there is also clear evidence of sediment slumping and reworking throughout the tunnel. The reworking of the loess deposits in the CPT offers an explanation for the variability in ages obtained from organic material within foliations of wedge 50S. Similar variability in magnetic susceptibility studies in the Fairbanks region and the CPT has been attributed to this reworking of sediments (e.g. Beget et al., 1990). Under periglacial conditions, solifluction of the active layer during summer months transports lobes of sediment downslope (French, 2008). Warm climates instigate thawing of permafrost and ground ice, promoting reworking of sediments by slope wash and mixing by roots from forest cover. These processes can result in the emplacement of older sediments above younger surfaces. Sediment from the soil surface that is incorporated into an ice wedge forming on a slope, as is the case at the CPT, is thus likely to be older than the ice containing it. The dates obtained from organic material in wedge 50S cannot conclusively be considered contemporaneous with the ice in which it is entrained. Rather, the ages represent periods of organic matter production, likely during warmer climates prior to ice wedge formation. This older organic material is likely to have been incorporated into the ice wedge via sediment mass transport from higher elevations, falling into thermal contraction cracks below.

The measured radiocarbon ages of the sediment are considered to be relatively unaffected by contamination from both infinitely old and modern carbon. Contamination of an organic sample by either old or modern organic material can result in radiocarbon dates that do not represent the true age of sediments being dated. Reworking of sediments above the ice wedge may have resulted in contamination with older material, however introduction of infinitely old carbon to a sample with no detectable ^{14}C has less of an effect on the apparent age of a sample than introduction of modern carbon with higher ^{14}C activity (Olsson, 1991; Taylor, 1987). For example, for a sample with an actual age of 30 ka, 5% contamination with modern carbon would produce an apparent age of 20 ka, 1% with an age of 25 ka, and 0.5% with an age of 27 ka (Olsson, 1991). A 30 kyr old sample with 5% contamination by 50 kyr old material (i.e. material 20 kyr older than the true age) would yield a date of 30.4 ka, or 400 years too old (Taylor, 1987). One percent contamination by older carbon would yield a date approximately 50 years too old, and smaller fractions are practically undetectable. The samples selected for dating from wedge 50S contained 4.0 – 52.5 mg of combusted carbon. 5 % of those samples would result in 0.2 – 2.6 mg of carbon present in the sample to create an apparent age that was too young. These levels of modern carbon are not considered to be present in the samples from 50S, as precautions were taken during the sampling process to prevent such contamination, and none observed upon visual inspection.

Katayama et al. (2007) obtained a ^{14}C date of 29.8 cal kyr BP from wedge 50S by dating of CH_4 inclusions in air bubbles within the ice. Their date falls within the range of dates I obtained in this study of 28.3 to 37.0 cal kyr BP. Magnetic susceptibility records from loess deposits from the Halfway House section west of Fairbanks, correlated to the

Goldstream Valley loess deposit 1 km south of the CPT, display a zone of oscillating magnetic susceptibility, indicating sudden changes from warm to cool climates. Beget (1990) suggested that the Halfway House section can be correlated to the section within the CPT dated from 31 – 35 ka by Hamilton et al. (1988). The section of silt in the Halfway House and Goldstream Valley deposits is overlain by a loess deposit containing little organic matter and characterized by larger grain sizes and higher magnetic susceptibility, indicative of glacial conditions. Beget (1990) considered these deposits to be Late Wisconsinan in age. More definitive conclusions regarding the ages of the Goldstream Formation await more accurate radiocarbon ages from the sediments and ground ice.

I conclude that the section of the Goldstream Formation exposed within the CPT and containing wedge 50S was deposited during the climatically variable period from 31 – 35 ka, when interstadials 5-7 rapidly brought warm temperatures across the Northern Hemisphere (Dansgaard et al., 1993). Radiocarbon samples R1, R10, R14, and R18 fall during the time Greenland was experiencing D-O events (Figure 16). Following this period, climate became colder during Heinrich event 3, and there was an absence of D-O events. Sample R6 (28.3 cal ka) and the methane sample (~29 cal ka) dated by Katayama et al. (2007) dated to around the time of Heinrich Event 3, which was estimated to be 31 ka (Hemming, 2004). The variation in $\delta^{18}O$ values from 50S is 5.95‰, which is similar to stable isotope variations recorded in Greenland ice from interstadial 5 to the following cold interval defined by Heinrich event 3 (Bond et al., 1999; Wang et al., 2001) (Figure 17). The ~6‰ change in $\delta^{18}O$ in wedge 50S is also strikingly similar to the 6‰ change in $\delta^{18}O$ documented in the Barrow ice wedge system during the Younger Dryas cold event

(Meyer et al., 2010), suggesting that the magnitude of cooling at the CPT was similar to that occurring during the Younger Dryas at the much higher latitude of 70°N.

I propose the following scenario for growth of ice wedge 50S: during Heinrich event 3, when temperatures were extremely low, thermal contraction cracking was initiated and wedge 50S grew. This event may be the same cooling suggested by Beget et al. (1990) in the Fairbanks region loess, interpreted from an increase in magnetic susceptibility and grain size, and a decrease in organic matter. Radiocarbon sample R6 (28.3 cal kyr BP), as well as the methane sample dated by Katayama et al. (2007) (29.8 cal kyr BP) from within the wedge, falls shortly after Heinrich event 3; they both date to a time when $\delta^{18}O$ values, and therefore temperatures, were very low, immediately preceding interstadial 4 in Greenland. The approximate age of 31 kyr BP for Heinrich event 3 is uncertain. That age is based on correlations between ice core records and sediment cores; the exact timing is estimated to have occurred within approximately 1000 years of that date (Hemming, 2004). The two samples that fall younger than 31 ka, therefore, may have formed before or during Heinrich event 3. The sudden climatic amelioration which caused 50S to stop growing in the middle of a cool, stable period may be interstadial 4. There was a short cool period following interstadial 4, during which the thin vein of ice that penetrates the top of 50S on the right side may have formed. The top of the ice wedge may have eroded during a subsequent warming, such as during interstadial 3.

The T – $\delta^{18}O$ relationship from GNIP stations in Alaska and nearby regions can be utilized to estimate the magnitude of the temperature change represented by the change in $\delta^{18}O$ recorded by wedge 50S. The resultant linear regression equation from the T – $\delta^{18}O$ relationship from records at each GNIP station indicates the change in $\delta^{18}O$ that is

predictable from a 1°C fluctuation in temperature (Table 4). The stable isotopic values in each foliation are interpreted to represent homogenized or mean winter precipitation $\delta^{18}O$ and δD values.

The GNIP station with the highest R^2 value with a similar continental climate as the CPT is Mayo, where 90% of the total variation in $\delta^{18}O$ can be explained by the temporal linear relationship between temperature and $\delta^{18}O$ as described by the regression equation $\delta^{18}O(‰) = 0.28 \times T(°C) - 21.60$, which corresponds to a 21.3°C change in temperature (Table 4). This large temperature variation exceeds estimates of ~10ºC for the warm to cold transition out of D-O events. GNIP stations in Whitehorse and Yellowknife indicate a high correlation between $\delta^{18}O$ and temperature, with calculated temperature changes of 35°C and 27°C, respectively. These stations have a similar geography and continental

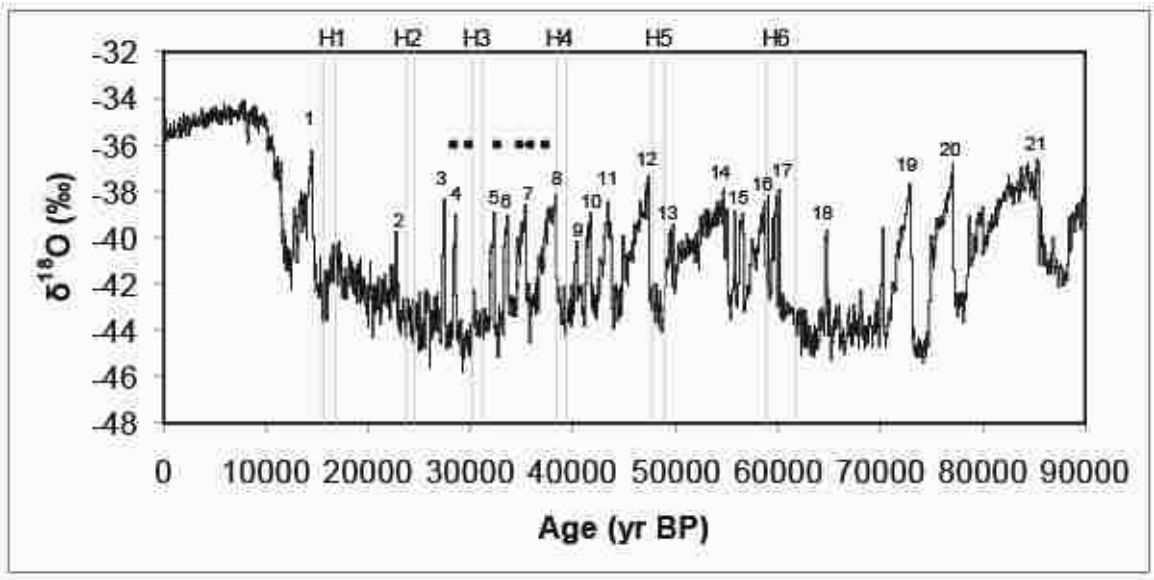

Figure 16. $\delta^{18}O$ record from NGRIP with 50-year resolution on the GICC05 timescale. Numbers 1-21 identify ice core interstadials associated with D-O events; gray lines labeled H1-H6 are Heinrich events as dated by Wang et al. (2001). Black dots are radiocarbon dates obtained from 50S for this study and by Katayama et al. (2007), samples from left to right are R6, Katayama et al. (2007) date, R1, R18, R10, and R14.

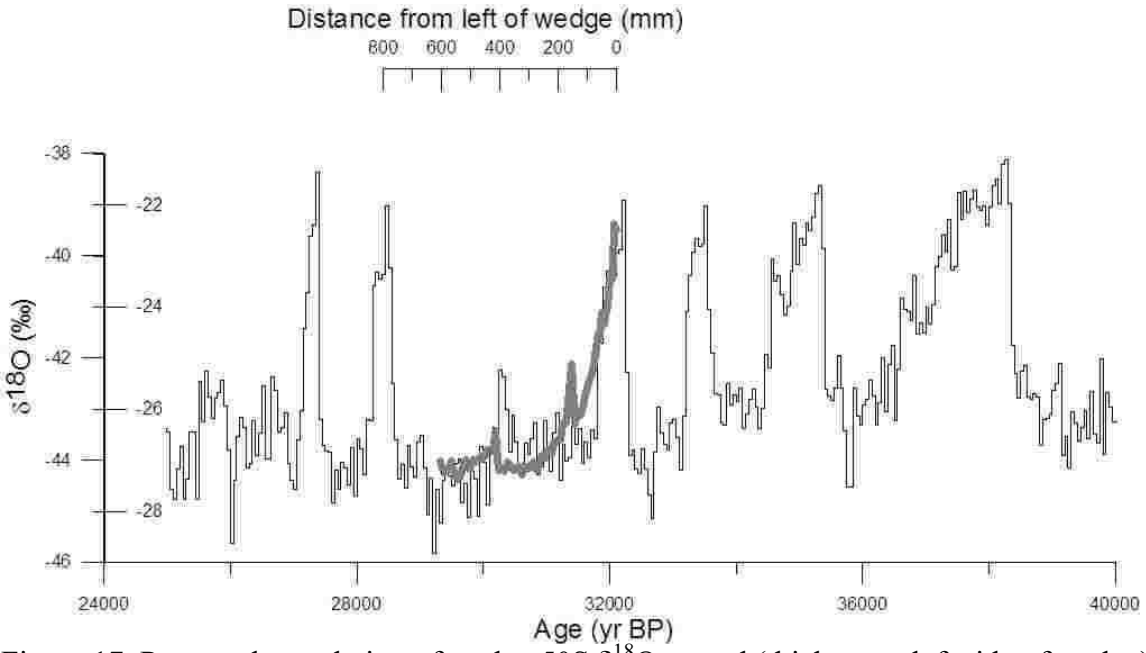

Figure 17. Proposed correlation of wedge 50S $\delta^{18}O$ record (thick gray; left side of wedge) to the NGRIP 50-year ice core record on the GICC05 timescale (thin gray) (Andersen et al., 2005; Svennson et al., 2006)

climate as the CPT, as precipitation reaching these locations experiences rainout over the large mountain ranges the air masses cross on their track to the interior of the continent. The correlation between temperature and $\delta^{18}O$ for Adak is not statistically significant, as shown by the extremely low R^2 value for the linear regression calculated for those variables, as well as the implausible change in temperature of 302°C calculated for the measured 5.95‰ change in $\delta^{18}O$ in wedge 50S. This may be due to Adak's location on an island in the Aleutian arc, where the surrounding ocean moderates climate, and $\delta^{18}O$ values are more closely related to conditions in the original moisture source. Inuvik, near the Canadian Arctic coast, also has a low R^2 value of 0.37, with a lower interpreted temperature change in 50S of 12°C.

Table 4. Linear regression data indicating the ‰ change in $\delta^{18}O$ per 1°C change in temperature from each GNIP station. Temperature changes for the 5.95 ‰ variation in $\delta^{18}O$ measured in 50S as calculated from each linear regression are also provided.

	Adak	Barrow	Bethel	Inuvik	Mayo	Whitehorse	Yellowknife	Spatial (All)	Spatial (Winter)
$\Delta\delta^{18}O/\Delta T$	0.02	0.26	0.18	0.49	0.28	0.17	0.22	0.73	0.78
R^2	0.01	0.69	0.78	0.37	0.90	0.49	0.85	0.23	0.62
T change (°C) for 5.95 ‰ change in $\delta^{18}O$	301.52	22.97	33.42	12.20	21.34	35.32	27.02	7.83	7.33

A temperature change in winter temperatures of 21-35°C is not suggested or inferred for other paleoclimate records from this time, as most D/O events are characterized by temperature changes of approximately 10°C. The temperature change of 8.6°C calculated using the spatial Dansgaard (1964) T – $\delta^{18}O$ relationship is consistent with the magnitude of temperature change between the interstadials of D-O events and the cool Heinrich events. The spatial $\delta^{18}O$/temperature gradient for all Alaska and Yukon stations using mean monthly temperature and $\delta^{18}O$ values from all months results in a $\delta^{18}O/^{o}C$ gradient of 0.73‰, which applied to the change in wedge 50S $\delta^{18}O$ suggests a total change in temperature of 7.8°C (Table 4). When the spatial relationship is calculated using temperature and $\delta^{18}O$ values from all stations, but only during winter months, a slope of 0.78‰/°C was calculated, resulting in a change of temperature of 7.33°C recorded in 50S. The temperature variations estimated using these spatial T – $\delta^{18}O$ relationships are similar to a cooling from a D-O interstadial into a Heinrich event. A change in winter temperatures of this magnitude is enough to promote the continual growth of ice wedges, and is a probable event considering temperature changes documented around the globe at that time.

CHAPTER 6

CONCLUSIONS

As modern climate continues to warm along with a rise in greenhouse gases, understanding the response of sensitive high-latitude regions has become increasingly important. The effect of rapid climate change on periglacial environments can be evaluated by looking at past events, such as the rapid and large-scale D-O events during MIS 3. Late Quaternary relict ground ice in the CPT is a unique proxy, recording cooling in events with the growth of ice wedges and aggrading permafrost, and warming events with erosional and slumping features.

Wedge 50S from the CPT provides a unique record of Late Pleistocene climate variability in a continental sub-Arctic environment. I forward four conclusions from this study. First, the stable isotope record indicates that a climatic cooling is recorded in the wedge ice, signified by a 5.95‰ decrease in $\delta^{18}O$ values, correlative to the transition from the warm D-O interstadials 5 – 7 to Heinrich event 3. Second, the magnitude of the cooling is approximately 7.3°C, estimated using modern winter precipitation values from GNIP stations in Alaska and Western Canada. Third, the age of the sediments in the ice is not necessarily contemporaneous with the age of the frozen snowmelt containing them, so radiocarbon ages from within the wedge may be from sediment that aggraded during the warm interstadials. Lastly, wedge 50S formed epigenetically during the cold climate of Heinrich event 3.

Future work investigating the response of permafrost and sub-Arctic climate to rapid climate change during MIS 3 should involve stable isotopic analysis of additional ice wedges and other ground ice within the CPT, to test if a similar magnitude decrease in

$\delta^{18}O$ values of winter precipitation is measured at the same stratigraphic position. Massive ice in the CPT records changes in temperature, however for ice wedges to serve as reliable climate proxies, the material dated must clearly be the same age as the ice it is contained within. Because organic material in foliations within the wedge may be older than the ice, more reliable dates could potentially be obtained by dating ^{14}C in CO_2 captured in air bubbles within the ice.

APPENDIX

SUPPLEMENTAL DATA

Ice Wedge Stable Isotopes

Sample ID	Avg. Distance from left edge of wedge (cm)	δD (‰, V-SMOW)	$\delta^{18}O$ (‰, V-SMOW)	*d*
50S-1A	behind sample 50S-1	-174.3	-22.4	5.2
50S-1B	behind sample 50S-2	-171.9	-22.4	7.0
50S-1	2.5	-179.5	-22.9	3.5
50S-2	7.5	-179.5	-22.8	2.8
50S-3	12.5	-186.3	-23.6	2.2
50S-4	17.5	-186.1	-23.6	2.8
50S-5	22.5	-186.1	-23.9	4.7
50S-6	32.5	-188.3	-24.4	7.2
50S-7	37.5	-190.7	-24.6	6.5
50S-8	42.5	-191.1	-24.8	7.4
50S-9	47.5	-192.6	-24.8	5.7
50S-10	52.5	-193.1	-24.5	2.6
50S-11	57.5	-195.9	-25.1	5.0
50S-12	62.5	-193.6	-24.9	5.6
50S-13	67.5	-197.1	-25.1	3.3
50S-14	72.5	-198.1	-25.4	5.5
50S-15	77.5	-196.7	-25.6	8.2
50S-16	85	-198.7	-25.8	7.4
50S-17	95	-198.7	-25.9	8.7
50S-18	105	-201.0	-26.2	8.6
50S-19	115	-202.9	-26.5	8.9
50S-20	125	-204.6	-26.6	8.5
50S-21	135	-203.9	-26.6	8.9
50S-22	145	-204.6	-26.8	9.7
50S-23	155	-200.3	-25.2	1.4
50S-24	165	-199.5	-26.2	10.0
50S-25	175	-200.2	-26.6	12.8
50S-26	185	-203.7	-26.6	9.2
50S-27	195	-203.3	-26.9	11.8
50S-28	205	-204.2	-26.9	11.1
50S-29	215	-202.6	-27.0	13.4
50S-30	225	-203.8	-27.2	14.1
50S-31	235	-204.5	-27.1	12.1
50S-32	245	-206.1	-27.3	12.1
50S-33	255	-204.6	-27.2	13.2
50S-34	265	-205.0	-27.3	13.6
50S-35	275	-203.3	-27.5	16.4
50S-36	285	-205.7	-27.3	13.0
50S-37	295	-204.8	-27.4	14.2
50S-38	305	-206.3	-27.4	13.1
50S-39	315	-203.8	-27.4	15.7
50S-40	325	-205.1	-27.7	16.7
50S-41	335	-203.3	-27.4	16.1

Sample ID	Avg. Distance from left edge of wedge (cm)	δD (‰, V-SMOW)	$\delta^{18}O$ (‰, V-SMOW)	*d*
50S-42	345	-205.9	-27.5	14.0
50S-43	355	-205.1	-27.5	14.8
50S-44	365	-205.9	-27.5	13.9
50S-45	375	-206.6	-27.3	12.1
50S-46	385	-203.4	-27.6	17.1
50S-47	395	-205.2	-27.5	14.6
50S-48	405	-203.7	-27.4	15.9
50S-49	415	-208.5	-27.5	11.8
50S-50	425	-209.3	-28.0	14.3
50S-51	435	-206.7	-28.0	16.9
50S-52	445	-208.4	-28.0	15.9
50S-53	455	-209.2	-28.1	15.3
50S-54	465	-209.4	-28.1	15.4
50S-55	475	-209.1	-28.1	15.5
50S-56	485	-208.3	-28.1	16.4
50S-57	495	-208.5	-28.3	17.9
50S-58	505	-208.2	-28.0	15.9
50S-59	515	-211.1	-28.2	14.6
50S-60	525	-210.2	-28.5	17.9
50S-61	535	-209.5	-28.5	18.2
50S-62	545	-208.0	-28.4	19.2
50S-63	555	-208.0	-28.1	16.9
50S-64	565	-208.7	-28.4	18.1
50S-65	575	-206.8	-28.3	19.7
50S-66	585	-209.0	-28.4	18.1
50S-67	595	-208.1	-28.1	17.0
50S-68	605	-210.3	-28.4	16.7
50S-69	615	-207.2	-28.1	17.8
50S-70	625	-207.9	-27.8	14.4
50S-71	635	-208.2	-28.1	16.6
50S-72	645	-208.1	-28.2	17.4
50S-73	655	-209.6	-28.4	17.5
50S-74	665	-206.6	-28.4	20.7
50S-75	675	-204.8	-27.2	12.9
50S-76	685	-205.0	-27.6	15.8
50S-77	695	-204.4	-27.5	15.9
50S-78	705	-205.8	-27.6	15.2
50S-79	715	-204.9	-27.7	16.7
50S-80	725	-205.1	-27.6	15.4
50S-81	735	-204.6	-27.5	15.6
50S-82	745	-205.5	-27.7	16.0
50S-83	755	-205.9	-27.7	15.8
50S-84	765	-204.7	-27.7	17.2
50S-85	775	-203.2	-27.8	19.0
50S-86	785	-204.0	-28.1	20.5
50S-87	795	-206.5	-28.2	19.1
50S-88	805	-204.5	-28.1	20.1
50S-89	815	-200.9	-27.5	19.3
50S-90	825	-203.8	-27.6	17.3
50S-91	835	-203.0	-27.6	18.0

Sample ID	Avg. Distance from left edge of wedge (cm)	δD (‰, V-SMOW)	$\delta^{18}O$ (‰, V-SMOW)	*d*
50S-92	845	-203.8	-27.9	19.1
50S-93	855	-204.5	-27.8	18.3
50S-94	865	-205.2	-27.9	17.6
50S-95	875	-202.8	-27.5	17.6
50S-96	885	-203.8	-27.6	17.0
50S-97	895	-204.5	-27.5	15.5
50S-98	905	-205.1	-27.3	13.0
50S-99	915	-207.2	-26.8	7.4
50S-100	925	-205.6	-26.4	5.8
50S-101	935	-205.4	-26.5	6.9
50S-102	945	-205.3	-26.4	5.8
50S-103	955	-206.4	-26.5	5.3
50S-104	965	-205.7	-26.5	6.3
50S-105	975	-205.8	-26.5	6.2
50S-106	985	-206.9	-26.5	5.3
50S-107	995	-204.9	-26.5	7.2
50S-108	1005	-203.9	-26.7	9.4
50S-109	1015	-205.2	-26.6	7.5
50S-110	1025	-204.2	-26.8	10.3
50S-111	1035	-204.4	-26.2	5.5
50S-112	1045	-205.4	-26.2	4.4
50S-113	1055	-204.4	-26.3	6.1
50S-114	1065	-206.0	-26.4	5.3
50S-115	1075	-204.4	-26.6	8.5
50S-116	1085	-202.5	-26.3	7.6
50S-117	1095	-202.8	-26.2	7.1
50S-118	1105	-201.7	-26.0	6.0
50S-119	1115	-202.4	-26.1	6.3
50S-120	1125	-201.0	-25.9	6.0
50S-121	1135	-198.5	-25.8	7.8
50S-122	1145	-198.2	-25.7	7.4
50S-123	1155	-199.4	-25.6	5.4
50S-124	1165	-197.9	-26.1	10.6
50S-125	1175	-195.2	-25.7	10.6
50S-126	1185	-193.3	-25.8	12.9
50S-127	1195	-193.4	-25.3	9.3
50S-128	1205	-192.1	-25.2	9.3
50S-129	1215	-190.3	-25.0	9.8
50S-130	1225	-193.4	-25.3	9.3
50S-131	1235	-192.1	-25.2	9.3
50S-132	1245	-190.3	-25.0	9.8

High Resolution Ice Wedge Stable Isotopes

Sample ID	Avg. Distance from left edge of wedge (cm)	δD (‰, V-SMOW)	$\delta^{18}O$ (‰, V-SMOW)	*d*
5050901	126	-198.0	-24.5	-2.2
5050902	128	-197.1	-24.3	-2.5
5050903	130	-198.1	-24.7	-0.8
5050904	132	-201.1	-25.1	-0.5
5050905	134	-198.4	-24.8	0.2
5050906	136	-200.3	-24.9	-0.8
5050907	138	-197.3	-24.4	-2.2
5050908	140	-200.5	-25.0	-0.5
5050909	142	-201.9	-25.1	-1.2
5050910	144	-200.6	-24.9	-1.4
5050911	146	-202.4	-25.2	-0.5
5050912	148	-201.3	-25.0	-1.1
5050913	150	-202.4	-25.2	-0.7
5050914	152	-202.7	-25.3	-0.3
5050915	154	-203.2	-25.3	-0.4
5050916	156	-203.0	-25.3	-0.6
5050917	158	-202.4	-25.2	-0.5
5050918	160	-203.7	-25.4	-0.7
5050919	162	-200.6	-24.9	-1.8
5050920	164	-204.1	-25.6	0.5
5050921	166	-203.9	-25.5	0.2
5050922	168	-203.6	-25.5	0.5
5050923	170	-204.5	-25.7	1.3
5050924	172	-203.6	-25.1	-2.5
5050925	174	-205.0	-25.7	0.8
5050926	176	-199.4	-24.6	-2.6
5050927	178	-205.0	-25.5	-0.7
5050928	180	-205.2	-25.7	0.3
5050929	182	-203.7	-25.5	0.3
5050930	184	-205.3	-25.7	-0.1
5050931	186	-204.9	-25.7	0.6
5050932	188	-205.1	-25.6	-0.5
5050933	190	-205.4	-25.7	0.1
5050934	192	-204.2	-25.6	0.6
5050935	194	-206.5	-25.9	0.9
5050936	196	-205.9	-25.6	-1.0
5050937	198	-205.9	-25.8	0.7
5050938	200	-205.9	-25.9	1.1
5050939	202	-205.9	-25.6	-0.9
5050940	204	-205.7	-25.7	-0.4
5050941	206	-206.2	-25.6	-1.3
5050942	208	-205.9	-25.9	0.9
5050943	210	-204.3	-25.6	0.2
5050944	212	-206.6	-25.9	0.5
5050945	214	-205.5	-25.9	1.4
5050946	216	-206.4	-25.8	0.1
5050947	218	-205.8	-25.7	0.1
5050948	220	-206.8	-26.0	0.9

Surface Water Stable Isotopes

Sample ID	Location	δD (‰, V-SMOW)	$\delta^{18}O$ (‰, V-SMOW)
AK-1	Fairbanks	-151.43	-20.71
AK-2	Fairbanks	-146.18	-19.65
AK-3	Fairbanks	-166.64	-22.93
AK-4	Fairbanks	-125.82	-17.42
AK-5	Fairbanks	-126.48	-17.94
RD-1	Red Dog	-125.41	-17.64
RD-2	Red Dog	-125.64	-17.41
RD-3	Red Dog	-121.37	-16.84
RD-4	Red Dog	-122.77	-17.09
RD-5	Red Dog	-125.22	-17.28
RD-6	Red Dog	-155.57	-21.29
RD-7	Red Dog	-152.44	-20.56

REFERENCES

Andersen, K.K., Svensson, A., Johnsen, S.J., Rasmussen, S.O., Bigler, M., Rothlisberger, R., Ruth, U., Siggaard-Andersen, M.L., Steffensen, J.P., Dahl-Jensen, D., Vinther, B.M., and Clausen, H.B., 2005, The Greenlland Ice Core Chronology 2005, 15-42 ka. Part 1: Constructing the time scale: Quaternary Science Reviews, v. 25.

Anderson, P. M., Bartlein, P. J., and Brubaker, L. B., 1994, Late Quaternary History of Tundra Vegetation in Northwestern Alaska: Quaternary Research, v. 41, p. 306-315.

Anderson, P. M., and Brubaker, L. B., 1994, Vegetation history of Northcentral Alaska: A mapped summary of late-Quaternary pollen data: Quaternary Science Reviews, v. 13, p. 71-92.

Anderson, P. M., Edwards, M. E., and Brubaker, L. B., 2004, Results and paleoclimate implications of 35 years of paleoecological research in Alaska, in Gillespie, A. R., Porter, S. C., and Atwater, B. F., eds., Developments in Quaternary Science: Amsterdam, Elsevier, p. 427-440.

Anisimov, O. A., Vaughan, D. G., Callaghan, T. V., Furgal, C., Marchant, H., Prowse, T. D., Vilhjalmsson, H., and Walsh, J. E., 2007, Polar Regions (Arctic and Antarctic), in Parry, M. L., Canziani, O. F., Palutikof, J. P., van der Linden, P. J., and Hanson, C. E., eds., Climate Change 2007: Impacts, Adaptation and Vulnerability. Contribution of Working Group II to the Fourth Assessment Report of the International Panel on Climate Change: Cambridge, Cambridge University Press, p. 653-685.

Asmerom, Y., Polyak, V. J., and Burns, S. J., 2010, Variable winter moisture in the southwestern United States linked to rapid glacial climate shifts: Nature Geoscience, v. 3, p. 114-117.

Axford, Y., Briner, J. P., Cooke, C. A., Francis, D. R., Michelutti, N., Miller, G. H., Smol, J. P., Thomas, E. K., Wilson, C. R., and Wolfe, A. P., 2009, Recent changes in a remote Arctic lake are unique within the past 200,000 years: Proceedings of the National Academy of Sciences, v. 106, no. 44, p. 18443-18446.

Beget, J., 1990, Middle Wisconsinan Climate Fluctuations Recorded in Central Alaska Loess: Geographie physique et Quaternaire, v. 44, no. 1, p. 3-13.

Beget, J. E., 1996, Tephrochronology and Paleoclimatology of the Last Interglacial - Glacial Cycle Recorded in Alaskan Loess Deposits: Quaternary International, v. 34-36, p. 121-126.

Beget, J. E., Stone, D. B., and Hawkins, D. B., 1990, Paleoclimatic forcing of magnetic susceptibility variations in Alaskan loess during the late Quaternary: Geology, v. 18, p. 40-43.

Behl, R. J., and Kennett, J. P., 1996, Brief interstadial events in the Santa Barbara basins, NE Pacific, during the past 60kyr: Nature, v. 379, p. 243-246.

Bond, G., Broecker, W., Johnsen, S., McManus, J., Labeyrie, L., Jouzel, J., and Bonani, G., 1993, Correlations between climate records from North Atlantic sediments and Greenland ice: Nature, v. 365, p. 143-147.

Bond, G., and Lotti, R., 1995, Iceberg Discharges into the North Atlantic on Millennial Time Scales During the Last Glaciation: Science, v. 267, p. 1005-1010.

Bond, G., Showers, W., Elliot, M., Evans, M., Lotti, R., Hajdas, I., Bonani, G., and Johnson, S., 1999, The North Atlantic's 1-2 kyr Climate Rhytym: Relation to Heinrich Events, Dansgaard/Oeschger Cycles and the Little Ice Age.

Bray, M. T., French, H. M., and Shur, Y., 2006, Further Cryostratigraphic Observations in the CRREL Permafrost Tunnel, Fox, Alaska: Permafrost and Periglacial Processes, v. 17, p. 233-243.

Brigham-Grette, J., Melles, M., and Minyuk, P., 2007, Overview and significance of a 250 ka paleoclimate record from El'Gygytgyn Crater Lake, NE Russia: Journal of Paleolimnology, v. 37, p. 1-16.

Briner, J. P., Kaufman, D. S., Manley, W. F., Finkel, R. C., and Caffee, M. W., 2005, Cosmogenic exposure dating of late Pleistocene moraine stabilization in Alaska: Geological Society of America Bulletin, v. 117, no. 7/8, p. 1108-1120.

Broecker, W.S., Kennett, J.P., Flower, B.P., Teller, J.T., Trumbore, S., Bonani, G., and Woelfli, W., 1989, Routing of meltwater from the Laurentide ice sheet during the Younger Dryas cold episode: Nature, v. 341, no. 6240, p. 318-321).

Broecker, W. S., Bond, G., and Klas, M., 1990, A salt oscillator in the glacial Atlantic? 1. The concept: Paleoceanography, v. 5, no. 4, p. 469-477.

Calkin, P. E., 1988, Holocene glaciation of Alaska (and adjoining Yukon Territory, Canada): Quaternary Science Reviews, v. 7, p. 159-184.

Clark, I., and Fritz, P., 1997, Environmental Isotopes in Hydrogeology: Boca Raton, Lewis Publishers, 328 p.

Cosford, J., Quing, H., Yuan, D., Zhang, M., Holmden, C., Patterson, W., and Hai, C., 2008, Millennial-scale variability in the Asian monsoon: Evidence from oxygen isotope records from stalagmites in southeastern China: Palaeogeography, Palaeoclimatology, Palaeoecology, v. 266, p. 3-12.

Dansgaard, W., 1964, Stable isotopes in precipitation: Tellus, v. 16, no. 4, p. 436-468.

Dansgaard, W., Johnsen, S., Clausen, H. B., Dahl-Jensen, D., Gundestrup, N. S., Hammer, C. U., Hvidberg, C. S., Steffensen, J. P., Sveinbjornsdottir, A. E., Jouzel, J., and Bond, G., 1993, Evidence for general instability of past climate from a 250-kyr ice-core record: Nature, v. 364, p. 218-220.

Eisner, W. R., and Colinvaux, P. A., 1990, A Long Pollen Record from Ahaliorak lake, Arctic Alaska: Review of Palaeobotony and Palynology, v. 63, p. 35-52.

Ferrians, O., 1998, Permafrost map of Alaska, USA: National Snow and Ice Data Center/World Data Center for Glaciology.

French, H. M., 2007, The Periglacial Environment: Hoboken, John Wiley & Sons Ltd, 458 p.

-, 2008, Recent Contributions to the Study of Past Permafrost: Permafrost and Periglacial Processes, v. 19, p. 179-194.

Hamilton, T. D., Craig, J. L., and Sellmann, P. V., 1988, The Fox permafrost tunnel: A late Quaternary geologic record in central Alaska: Geological Society of America Bulletin, v. 100, p. 948-969.

Hare, K. F., and Hay, J. E., 1974, The Climate of Canada and Alaska, in Bryson, R. A., and Hare, K. F., eds., Climates of North America: World Survey of Climatology: Amsterdam, Elsevier Scientific Publishing Company, p. 49-134.

Harry, D. G., and Gozdzik, J. S., 1988, Ice wedges: growth, thaw transformation, and

palaeoenvironmental significance: Journal of Quaternary Science, v. 3, no. 1, p. 39-55.
Hemming, S. R., 2004, Heinrich events: Massive late Pleistocene detritus layers of the North Atlantic and their global climate imprint: Reviews of Geophysics, v. 42, p. 1-43.
Hendy, I. L., and Kennett, J. P., 1999, Latest Quaternary North Pacific surface-water responses imply atmosphere-driven climate instability: Geology, v. 27, no. 4, p. 291-294.
Hoefs, J., 1997, Stable isotope geochemistry: New York, Springer, 201 p.
Jouzel, J., Stievenard, M., Johnsen, S. J., Landais, A., Masson-Delmotte, V., Sveinbjornsdottir, A. E., Vimeux, F., von Grafenstein, U., and White, J. W. C., 2007, The GRIP deuterium-excess record: Quaternary Science Reviews, v. 26, p. 1-17.
Kaufman, D. S., Anderson, R. S., Hu, F. S., Berg, E., and Werner, A., 2010, Evidence for a variable and wet Younger Dryas in southern Alaska: Quaternary Science Reviews, v. 29, p. 1445-1452.
Kaufman, D. S., Porter, S. C., and Gillespie, A. R., 2004, Quaternary alpine glaciation in Alaska, the Pacific Northwest, Sierra Nevada, and Hawaii, in Gillespie, A. R., Porter, S. C., and Atwater, B. F., eds., The Quaternary Period in the United States: Amsterdam, Elsevier p. 77-103.
Kiefer, T., Sarnthein, M., Erlenkeuser, H., Grootes, P. M., and Roberts, A. P., 2001, North Pacific response to millennial-scale changes in ocean circulation: Paleoceanography, v. 16, no. 2, p. 179-189.
Kotilainen, A. T., and Shackleton, N. J., 1995, Rapid climate variability in the North Pacific Ocean during the past 95,000 years: Nature, v. 377, p. 323-326.
Lee, J., Feng, X., Faiia, A. M., Posmentier, E. S., Kirchner, J. W., Osterhuber, R., and Taylor, S., 2010, Isotopic evolution of a seasonal snowcover and its melt by isotopic exchange between liquid water and ice: Chemical Geology, v. 270, p. 126-134.
Mackay, J. R., 1992, The frequency of ice-wedge cracking (1967-1987) at Garry Island, western Arctic coast, Canada: Canadian Journal of Earth Sciences, v. 29, p. 236-248.
Meyer, H., Schirrmeister, L., Yoshikawa, K., Opel, T., Wetterich, S., Hubberten, H., and Brown, J., 2010, Permafrost evidence for severe winter cooling during the Younger Dryas in northern Alaska: Geophysical Research Letters, v. 37, p. 1-5.
Meyer, H., Yoshikawa, K., Schirrmeister, L., and Andreev, A., 2008, The Vault Creek Tunnel (Fairbanks Region, Alaska): A Late Quaternary Palaeoenvironmental Permafrost Record, Ninth International Conference on Permafrost: Fairbanks, AK.
Mock, C. J., Bartlein, P. J., and Anderson, P. M., 1998, Atmospheric circulation patterns and spatial climatic variations in Beringia: International Journal of Climatology, v. 10, p. 1085-1104.
Muhs, D. R., Ager, T. A., and Beget, J. E., 2001, Vegetation and paleoclimate of the last interglacial period, central Alaska: Quaternary Science Reviews, v. 20, p. 41-61.
Nikolayev, V. I., and Mikhalev, D. V., 1995, An Oxygen-Isotope Paleothermometer from Ice in Siberian Permafrost: Quaternary Research, v. 43, p. 14-21.

Olsson, I. U., 1991, Conventional Radiocarbon Dating and Some Problems of 14C Dating, in Goksu, H. Y., Oberhofer, M., and Regulla, D., eds., Scientific Dating Methods: Brussels, Kluwer Academic Publishers, p. 15-35.

Overland, J. E., Adams, J. M., and Bond, N. A., 1999, Decadal Variability of the Aleutian Low and Its Relation to High-Latitude Circulation: Journal of Climate, v. 12, p. 1542-1548.

Pewe, T. L., 1975, Quaternary Stratigraphic Nomenclature in Unglaciated Central Alaska, no. 862, p. 32.

Pewe, T. L., Berger, G. W., Westgate, J. A., Brown, P. M., and Leavitt, S. W., 1997, Eva Interglaciation Forest Bed, Unglaciated East-Central Alaska: Global Warming 125,000 Years Ago: Geological Soceity of America Special Paper, v. 319, p. 1-54.

Reimer, P. J., Baillie, M. G. L., Bard, E., Bayliss, A., Beck, J. W., Blackwell, P. G., Bronk Ramsey, C., Buck, C. E., Burr, G. S., Edwards, R. L., Friedrich, M., Grootes, P. M., Guilderson, T. P., Hajdas, I., Heaton, T. J., Hogg, A. G., Hughen, K. A., Kaiser, K. F., Kromer, B., McCormac, F. G., Manning, S. W., Reimer, R. W., Richards, D. A., Southon, J. R., Talamo, S., Turney, C. S. M., van der Plicht, J., and Weyhenmeyer, C. E., 2009, IntCal09 and Marine09 Radiocarbon Age Calibration Curves, 0-50,000 Years cal BP: Radiocarbon, v. 51, no. 4, p. 1111-1150.

Rozanski, K., Araguas-Araguas, L., and Gonfiantini, R., 1993, Isotopic Patterns in Modern Global Precipitation, in Swart, P. K., Lohmann, K. C., McKenzie, J. A., and Savin, S., eds., Climate Change in Continental Isotopic Records: Geophysical Monograph, p. 1-36.

Schultz, M., 2002, On the 1470-year pacing of Dansgaard-Oeschger warm events: Paleoceanography, v. 17, no. 2, p. 1-9.

Sellmann, P. V., 1967, Geology of the USA CRREL Permafrost Tunnel, Fairbanks, Alaska: U.S. Army CRREL Technicl Report v. 199, p. 22.

Sharp, Z., 2007, Principles of Stable Isotope Geochemistry: Upper Saddle River, Pearson Prentice Hall, 344 p.

Sharp, Z. D., Atudorei, V., and Durakiewicz, T., 2001, A rapid method for determinination of hydrogen and oxygen isotope ratios from water and hydrous minerals: Chemical Geology, v. 178, p. 197-210.

Shulski, M., and Wendler, G., 2007, The Climate of Alaska: Fairbanks, University of Alaska Press, 216 p.

Shur, Y., French, H. M., Bray, M. T., and Anderson, D. A., 2004, Syngenetic Permafrost Growth: Cryostratigraphic Observations from the CRREL Tunnel near Fairbanks, Alaska: Permafrost and Periglacial Processes, v. 15, p. 339-347.

Stuiver, M., and Reimer, P. J., 1993, Extended 14C database and revised CALIB radiocarbon calibration program: Radiocarbon, v. 35, p. 215-230.

Svensson, A., Andersen, K.K., Bigler, M., Clausen, H.B., Dahl-Jensen, D., Davies, S.M., Johnsen, S.J., Muscheler, R., Rasmussen, S.O., Rothlisberger, R., Steffensen, J.P., and Vinther, B.M., 2006, The Greenland Ice Core Chronology 2005, 15-42 ka. Part 2: Comparison to other records: Quaternary Science Reviews, v. 25.

Taylor, R. E., 1987, Radiocarbon Dating: An Archaeological Perspective: Orlando, Academic Press, Inc., 212 p.

Taylor, S., Feng, X., Kirchner, J. W., Osterhuber, R., Klaue, B., and Renshaw, C. E., 2001, Isotopic evolution of a seasonal snowpack and its melt: Water Resources Research, v. 37, no. 3, p. 759-769.

Vasil'chuk, Y. K., and Vasil'chuk, A. C., 1997, Radiocarbon Dating and Oxygen Isotope Variations in Late Pleistocene Syngenetic Ice-Wedges, Northern Siberia: Permafrost and Periglacial Processes, v. 8, p. 335-345.

Voelker, A. H. L., 2002, Global distribution of centennial-scale records for Marine Isotope Stage (MIS) 3: a database: Quaternary Science Reviews, v. 21, p. 1185-1212.

Wang, Y. J., Cheng, H., Edward, R. L., An, Z. S., Wu, J. Y., Shen, C.-C., and Dorale, J. A., 2001, A High-Resolution Absolute-Dated Late Pleistocene Monsoon Record from hulu Cave, China: Science, v. 294, p. 2345-2348.

Weber, F. R., 1986, Glacial Geology of the Yukon-Tanana Upland, in Hamilton, T. D., Reed, K. M., and Thorson, R. M., eds., Glaciation in Alaska - The geologic record: Anchorage, Alaska Geological Society, p. 79-98.

Wiles, G. C., Jacoby, G. C., Davi, N. K., and McAllister, R. P., 2002, Late Holocene glacier fluctuations in the Wrangell Mountains, Alaska: Geological Society of America Bulletin, v. 114, no. 7, p. 896-908.

Yoshikawa, K., and Hinzman, L. D., 2003, Shrinking Thermokarst Ponds and Groundwater Dynamics in Discontinuous Permafrost near Council, Alaska: Permafrost and Periglacial Processes, v. 14, p. 151-160.

VITA

Graduate College
University of Nevada, Las Vegas

Corinne Y. Griffing

Degrees:
Bachelor of Science, Geoscience, 2008
University of Nevada, Las Vegas

Special Honors and Awards:
Nevada NASA Space Grant Consortium Fellowship, 2009-2010 Academic Year
Geological Society of America Bruce L. "Biff" Reed Research Award, Spring 2009

Thesis Title: Pleistocene Climate in Alaska from Stable Isotopes in an Ice Wedge

Thesis Examination Committee:
Chairperson, Matthew Lachniet, Ph. D.
Committee Member, Daniel Lawson, Ph. D.
Committee Member, Ganqing Jiang, Ph. D.
Committee Member, Stephen Rowland, Ph. D.
Graduate Faculty Representative, Liam Frink, Ph. D.